

Electronic Thesis and Dissertation Repository

---

5-29-2017 12:00 AM

# In Vivo Magnetic Resonance Imaging Morphometry Measurements of Pulmonary Airspace Enlargement

Eric J. Lessard  
*The University of Western Ontario*

Supervisor  
Grace Parraga  
*The University of Western Ontario*

Graduate Program in Medical Biophysics  
A thesis submitted in partial fulfillment of the requirements for the degree in Master of Science  
© Eric J. Lessard 2017

Follow this and additional works at: <https://ir.lib.uwo.ca/etd>



Part of the [Medical Biophysics Commons](#)

---

## Recommended Citation

Lessard, Eric J., "In Vivo Magnetic Resonance Imaging Morphometry Measurements of Pulmonary Airspace Enlargement" (2017). *Electronic Thesis and Dissertation Repository*. 4559.  
<https://ir.lib.uwo.ca/etd/4559>

This Dissertation/Thesis is brought to you for free and open access by Scholarship@Western. It has been accepted for inclusion in Electronic Thesis and Dissertation Repository by an authorized administrator of Scholarship@Western. For more information, please contact [wlsadmin@uwo.ca](mailto:wlsadmin@uwo.ca).

## Abstract

Diffusion-weighted magnetic resonance imaging (MRI) provides unparalleled information and measurements of lung structure and function without the burden of ionizing radiation. In particular, diffusion-weighted MRI provides estimates of airspace enlargement, which is a hallmark characteristic of emphysema. MRI provides a way to measure *in vivo* mean-linear-intercept ( $L_m$ ) and this is a promising measurement for clinical evaluation of disease progression in patients with Alpha-1 Antitrypsin Deficiency (AATD) in which airspace enlargement begins early in life. As such, our objective was to evaluate MRI measurements of airspace enlargement in AATD patients and compare these measurements to ex-smokers with chronic obstructive pulmonary disease (COPD) and healthy never-smokers. We compared these measurements with standard clinical measurements provided by spirometry, plethysmography and computed tomography; we also demonstrated that MRI detected differences in disease severity in patients with clinically similar measurements.

(135/150 words)

## Keywords

Hyperpolarized  $^3\text{He}$  magnetic resonance imaging, Chronic obstructive pulmonary disease, Alpha-1 antitrypsin deficiency, diffusion-weighted imaging, lung microstructure, emphysema

## Co-Authorship Statement

The following thesis contains one manuscript. The manuscript was accepted for publication in *Academic Radiology*. As first author of the manuscript (**Chapter 2**), I was a significant contributor to all aspects of the study as well as manuscript preparation and submission. Specifically, this involved image analysis, interpretation of data, performing statistics and drafting/final approval of the manuscript. Dr. Grace Parraga, as the principal investigator and my supervisor, provided support and guidance and overall was responsible for the concept and experimental design of the study in addition to data interpretation, drafting and final revisions of the manuscript. She was the guarantor of the data integrity as well as responsible for Good Clinical Practice (GCP). Polarization of  $^3\text{He}$  gas was performed by Andrew Wheatley, David Tessier and Dante PI Capaldi. MRI acquisition was performed by Trevor Szekeres MRT and David Reese MRT.

**Chapter 2** is an original research article entitled “Pulmonary  $^3\text{He}$  Magnetic Resonance Imaging Biomarkers of Regional Airspace Enlargement in Alpha-1 Antitrypsin Deficiency” and was accepted to *Academic Radiology* on May 27, 2017. This manuscript was co-authored by Eric Lessard, Heather M Young, Dr. Anurag Bhalla, Dr. Damien Pike, Dr. Khadija Sheikh, Dr. David G McCormack, Dr. Alexei Ouriadov and Dr. Grace Parraga. As first author I contributed to manuscript preparation, interpretation of the data as well as data analysis. Heather Young provided assistance with data analysis, manuscript preparation and editing, provided interpretation of data and assisted with figure preparation. Dr. Anurag Bhalla contributed to manuscript preparation, clinical interpretation of the data and data analysis. Dr. Damien Pike and Dr. Khadija Sheikh assisted with the data analysis and data acquisition. Dr. David G McCormack provided clinical/physiological interpretation of the data and subject referral. Dr. Alexei Ouriadov provided morphometry model development and was responsible for assisting with data interpretation.

## **Acknowledgments**

First, I would like to acknowledge my supervisor Dr. Grace Parraga for providing me with opportunities which I otherwise would not have been afforded. She has constantly provided a strong role model and her guidance throughout my degree has been invaluable to me.

To the members of my advisory committee, Drs Maria Drangova, Aaron Ward and David G McCormack who have taken the time to provide insight and feedback on my growth as a student. For that I am truly grateful.

To my lab mates both past and present, Alexei Ouriadov for always helping me with my MRI and morphometry questions and providing your expertise throughout my entire degree. Dante Capaldi for truly being one of the nicest and most helpful people I've met. For always having time to assist me regardless of your schedule and for providing some of the most entertaining and thought provoking conversations I've experienced. Dave Reese for our chats about everything from MRI to purchasing houses which have made many aspects of my life much easier and more enjoyable. Fumin Guo for your constant positive attitude. Heather Young for your friendship and meticulous eye while editing my work. Khadija Sheikh for always pushing me to enjoy life. Whether it is climbing 70+ flights of stairs for charity or taking a bus trip late at night to see the Golden Gate Bridge. Without you I would have spent the last two years quite a bit more socially isolated. Lyndsey Reid-Jones for our countless discussions ranging from adoption of cats to costochondritis. Megan Fennema for your constant comedy and countless fun times whether it be at ISMRM or chatting during coffee time, and for pretending my jokes were funny when no one else would. Rachel Eddy, having someone to go through common milestones together has made them that much easier to obtain, you've provided support and encouragement at each one. As well as other lab mates for without them this would not have been possible: Andrea Kassay, Anurag Bhalla, Robert Cesare, and Sarah Svenningson.

To everyone at Robarts who has made this a memorable two years, Amy Schranz for providing strong friendship throughout my degree and spending countless time practicing my seminar with me. Anne Leaist for our talks about cats and life here at Robarts. Derek Gillies for being my graduate school catalyst and providing strong friendship throughout this entire time. Dickson Wong for our chats about low-carb diets and many other topics. Olivia Stanley for

pushing me to contact PhD supervisors and for your constant help as a critical eye whether it be critiquing my diffusion section or a single-lined email. Terenz Escartin for always giving me good clinical questions and for our chats about the gym. Tomi Nano for always rooting for my success and your kind words of encouragement. Lastly, to the Scholl group for their constant entertainment while I worked upstairs.

Most importantly, I would like to thank my fiancé Amanda and her family, Sandro, Josie, and Eric Kuti for their constant support and understanding throughout this entire process.

# Table of Contents

Abstract .....	ii
Co-Authorship Statement.....	iii
Table of Contents .....	vi
List of Tables .....	ix
List of Figures .....	x
List of Appendices .....	xi
List of Abbreviations .....	xii
1 INTRODUCTION .....	1
1.1 Motivation and Rationale.....	1
1.2 Lung Structure and Function .....	3
1.2.1 Conducting Zone.....	3
1.2.2 Respiratory Zone.....	3
1.2.3 The Alveoli .....	4
1.3 Chronic Obstructive Pulmonary Disease .....	5
1.3.1 Chronic Bronchitis .....	5
1.3.2 Emphysema.....	6
1.4 Alpha-1 Antitrypsin Deficiency.....	7
1.4.1 Biology.....	7
1.4.2 Liver Disease .....	8
1.4.3 Lung Disease.....	8
1.4.4 Augmentation Therapy .....	8
1.5 Clinical Measurements of Lung Disease .....	9
1.5.1 Spirometry.....	9
1.5.2 Lung Volumes and Capacities .....	10
1.5.3 Diffusing Capacity of the Lung for Carbon Monoxide .....	11

1.5.4	Six-Minute Walk Test.....	12
1.5.5	St. George’s Respiratory Questionnaire .....	12
1.6	X-Ray Computed Tomography.....	12
1.6.1	Theory.....	12
1.6.2	Pulmonary X-Ray Computed Tomography .....	13
1.7	Magnetic Resonance Imaging.....	14
1.7.1	Theory.....	14
1.7.2	Pulmonary Magnetic Resonance Imaging .....	15
1.8	Thesis Objectives .....	24
1.9	References.....	26
<b>2</b>	<b>Chapter 2: Pulmonary <sup>3</sup>He Magnetic Resonance Imaging Biomarkers of Emphysema in Alpha-1 Antitrypsin Deficiency.....</b>	<b>35</b>
2.1	Introduction.....	35
2.2	Materials and Methods.....	37
2.2.1	Study Volunteers and Design.....	37
2.2.2	Spirometry, Plethysmography, SGRQ and 6MWT .....	37
2.2.3	Image Acquisition.....	37
2.2.4	Image Analysis.....	38
2.2.5	Statistical Analysis.....	39
2.3	Results.....	40
2.4	Discussion.....	47
2.5	References.....	51
<b>3</b>	<b>Chapter 3: Conclusions and Future Directions .....</b>	<b>57</b>
3.1	Overview and Research Questions .....	57
3.2	Summary and Conclusions .....	57
3.3	Limitations .....	58

3.4	Future Directions .....	59
3.4.1	Overcoming Issues Related to Gas Dispersion .....	59
3.4.2	Accelerated Imaging .....	60
3.4.3	An Inevitable Transition to $^{129}\text{Xe}$ .....	60
3.4.4	Functional Diffusion Maps of the Lungs .....	61
3.4.5	Longitudinal Evaluation of AATD .....	63
3.5	Significance and Impact.....	64
3.6	References.....	64
4	Appendix .....	66



## List of Tables

Table 1-1: GOLD Severity Grades	5
Table 2-1: Demographic and pulmonary function measurements	40
Table 2-2: Pulmonary MRI and CT measurements	44
Table 2-3: MRI and CT Measurements by Participant	46

## List of Figures

Figure 1-1: Conducting and Respiratory Zones .....	4
Figure 1-2: Centriacinar and Panacinar Emphysema.....	6
Figure 1-3: Micro-CT Lung Images .....	7
Figure 1-4: Flow Volume Curve.....	10
Figure 1-5: Lung Volumes.....	11
Figure 1-6: CT Radiodensity and Histogram.....	14
Figure 1-7: <sup>1</sup> H Thorax image for representative NS, COPD and AATD Subjects.....	15
Figure 1-8: Static ventilation images for representative NS, COPD and AATD subjects .....	18
Figure 1-9: Diffusion-weighted Pulse Sequence .....	19
Figure 1-10: Diffusion sensitizing pulse gradient waveform .....	20
Figure 1-11: Non-Diffusion and Diffusion-weighted <sup>3</sup> He Ventilation Image .....	21
Figure 1-12: Static ventilation and ADC for AATD subject .....	21
Figure 1-13: Weibel representation of the acinar duct.....	23
Figure 1-14: Infinite cylinder geometry.....	23
Figure 2-1: Thoracic CT and MRI for Never-smokers, COPD and AATD Participants .....	41
Figure 2-2: Morphometry Maps for Representative Never-smokers, COPD ex-smokers and AATD Patients.....	43
Figure 2-3: Regional Imaging Biomarkers .....	45
Figure 3-1: Functional Diffusion Map Workflow .....	62
Figure 3-2: Longitudinal Evaluation of AATD .....	63

## List of Appendices

Appendix A - Permission for Reproduction of Scientific Articles .....	66
Appendix B - Health Science Research Ethics Board Approval Notices.....	67
Appendix C - Curriculum Vitae.....	73

## List of Abbreviations

6MWD	Six Minute Walk Distance
6MWT	Six Minute Walk Test
AATD	Alpha-1 Antitrypsin Deficiency
ADC	Apparent Diffusion Coefficient
AL	Apical Lung
ATS	American Thoracic Society
BL	Basal Lung
COPD	Chronic Obstructive Pulmonary Disease
CT	Computed Tomography
$D_0$	Free Diffusion Coefficient
$D_L$	Longitudinal Diffusion
$DL_{CO}$	Diffusion Capacity of the Lung for Carbon Monoxide
$D_T$	Transverse Diffusion
ERV	Expiratory Reserve Volume
ES	Ex-Smoker
$^{19}F$	Flourine-19
FD	Fourier Decomposition
FDM	Functional Diffusion Map
$FEV_1$	Forced Expiratory Volume in 1 Second
FGRE	Fast Gradient Recalled Echo
FOV	Field of View
FRC	Functional Residual Capacity
$G_m$	Gradient Maximum
$^1H$	Proton
$^3He$	Helium-3
HU	Hounsfield Units
IRV	Inspiratory Reserve Volume
L	Alveoli Length
LAC	Low Attenuation Clusters
$L_m$	Mean Linear Intercept
MANOVA	Multiple Analysis of Variance
MRI	Magnetic Resonance Imaging
NS	Never-Smoker
r	Internal Airway Radius
R	External Airway Radius
$RA_{950}$	Relative Area of the CT Density Histogram <-950 HU
RF	Radio Frequency
RV	Residual Volume
SGRQ	St. George's Respiratory Questionnaire
SPO <sub>2</sub>	Arterial Oxygenation
S/V	Surface-to-Volume Ratio
TE	Echo Time
TLC	Total Lung Capacity
TV	Tidal Volume
UTE	Ultrashort Echo Time
VC	Vital Capacity

VDP  
WL  
<sup>129</sup>Xe

Ventilation Defect Percentage  
Whole Lung  
Xenon-129

# 1 INTRODUCTION

*“Can one hear the shape of a drum?” - Mark Kac.<sup>1</sup> This simple question builds the foundation for this research. Can you listen to an MRI signal from the lung parenchyma and from that determine its shape and form? This introduction provides the required information as a prelude to the remaining chapters which explore this question across a range of lung disease.*

## 1.1 Motivation and Rationale

Chronic obstructive pulmonary disease (COPD) is a leading cause of death and hospitalizations worldwide.<sup>2</sup> It affects millions of people and has an incredible economic burden on the healthcare system in Canada.<sup>3</sup> The hallmark features of COPD include thickening of the bronchial walls, excessive mucus production and partial or complete destruction of the alveolar ducts and sacs.<sup>4</sup> This combination of factors leads to a decrease in pulmonary function and overall quality of life. Individuals with a diagnosis of Alpha-1 Antitrypsin Deficiency (AATD) lack a protein required for regulation of neutrophil elastase and as a result can rapidly develop a phenotype of COPD called emphysema.<sup>5</sup> Unfortunately, there is no cure for AATD and current treatment is expensive,<sup>6</sup> and has controversial efficacy with no improvements in exercise capacity or quality of life for the patient.<sup>7</sup> Emphysema is characterized by parenchymal destruction which results in overall airspace enlargement. This enlargement can be characterized by lung morphometry, the study of lung form. This can be used to quantify disease severity and progression regionally throughout the lung. The American Thoracic Society (ATS) and European Respiratory Society (ERS) joint task force consider quantification of lung structure to be the gold standard in evaluating clinical interventions, severity of disease and response to treatment.<sup>8</sup>

In the clinic, measurements of lung structure and function are made using a wide range of tools, from simple airflow measurements to complex three dimensional computed tomography (CT). Many of these tools will be outlined in further detail later in this chapter. Airflow measurements (spirometry) taken at the mouth can be used to quantify lung

function and airflow obstruction. Spirometry is the gold standard for diagnosis of chronic obstructive pulmonary disease. It is also possible to measure lung volumes which can give the volume of gas remaining in the lungs after full exhalation. The volume remaining at the end of exhalation (RV) as a ratio of total lung capacity (TLC) is a measurement of gas trapping. Diffusion tests can give an estimate of the ability for O<sub>2</sub> to diffuse across the alveolar-capillary membrane which is a quantity that is reduced in diseases such as emphysema. Measurements of lung structure and form can be performed using imaging techniques such as planar x-rays or by extending this to 3D x-ray CT. These techniques allow measurements of lung volumes and tissue density to be made but to truly measure the structure and form of the lung and the lung parenchyma, novel morphometry techniques must be employed to obtain measurements such as the surface-to-volume ratio and mean cord length.

Lung morphometry is not a new field. However, until recently, it relied on histology to provide 2D cross sections with which the overall 3D structure of the lungs are estimated.<sup>9,10</sup> In this method, an excised lung or section of the lung is sliced into 2D cross sections and through point counting, intersection counting and transect counting an estimation of lung volume, surface area or mean cord length can be made.<sup>9</sup> Unfortunately, this method relies on excised lung tissue thus limiting it to *ex-vivo* analysis.

Unfortunately, there are limited methods that provide accurate measurements of airspace size *in vivo*. Hyperpolarized noble-gas magnetic resonance imaging (MRI) provides an ionizing radiation free method of quantifying lung structure function *in vivo*. To accomplish this, diffusion-weighted MRI is employed, which measures the self-diffusion of the noble-gas molecules within the confinement of the lung parenchyma. Since the noble-gases used are biologically inert, this diffusion is related to the confining geometry, in this case that of the lung parenchyma. There has been much work done in measuring this confinement in the form of an apparent diffusion coefficient (ADC). Previous work in AATD measuring ADC,<sup>11-14</sup> relied on the single diffusion-weighted approach and did not extend to multiple diffusion-weights which can provide a more sensitive measurement of geometry. Recent work however, looked at a population of AATD subjects using different multiple diffusion-weighted modelling approaches but did so only for a single centre

coronal slice and without comparison to standard clinical measurements or regional evaluation.<sup>15</sup>

This thesis focuses on evaluation of alveolar destruction in COPD and AATD using multiple diffusion-weights, comparing these measurements to those used clinically such as spirometry and computed tomography as well as evaluating measurements of airspace enlargement regionally throughout the lung.

This thesis chapter will provide prerequisite knowledge to understand the original research presented in **Chapter 2**.

## 1.2 Lung Structure and Function

The primary function of the lungs is gas exchange. The lungs consist of branching generations (**Figure 1-1**) of bronchioles which ultimately end in the alveoli, where the majority of gas exchange occurs. The lungs can be divided into two sections, the conducting zone and the respiratory zone.

### 1.2.1 Conducting Zone

Beginning at the nose, the conducting zone is the first portion of the respiratory tract. This portion of the airways consists of those with the largest diameter with the main purpose of filtration, warming and transportation of incoming air. The conducting zone concludes at the terminal bronchioles. In the respiratory tract, the conducting zone consists of generations 1 to 16.

### 1.2.2 Respiratory Zone

The respiratory zone, generations 17 until the alveoli is the site of gas exchange in the lungs. This is the portion of the respiratory tract with the largest surface area which makes up the bulk of the lung parenchyma. This region of the lung consists primarily of the alveolar ducts, sacs and the alveoli. The alveoli are responsible for 90% of the gas exchange whereas the preceding respiratory bronchioles and alveolar ducts account for only 10%.



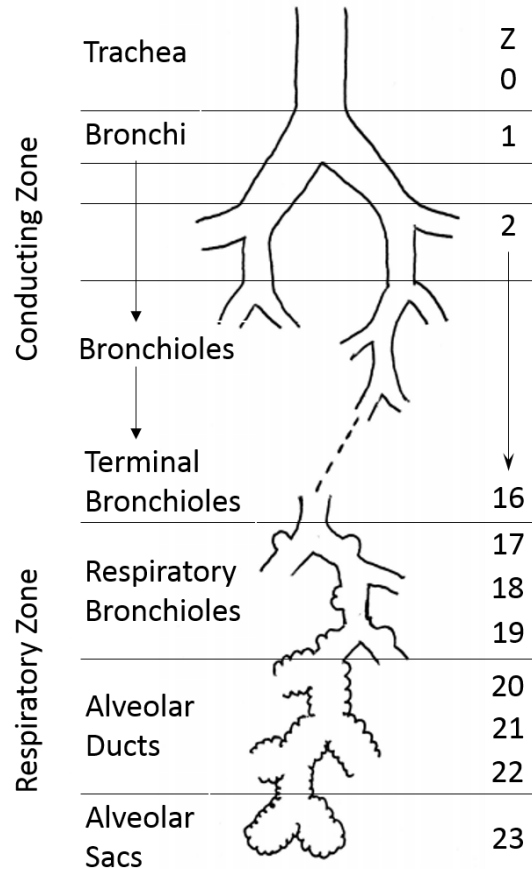


**Figure 1-1: Conducting and Respiratory Zones**

Respiratory tract generations (Z) with both conducting and respiratory zones beginning at the trachea (Z = 0) and ending at the alveoli (Z = 23). Adapted from West, JB, Respiratory Physiology: The Essentials, Ninth Edition.<sup>16</sup>

### 1.2.3 The Alveoli

The alveoli comprise the bulk of the lung parenchyma as they line the walls of the airways in the respiratory zone. Each alveolus is approximately 330  $\mu\text{m}$  in diameter<sup>16</sup> and the average adult has 480 million alveoli.<sup>17</sup> As a result of their small diameter and the vast number of alveoli, they have a surface area of roughly 70  $\text{m}^2$ .<sup>18</sup> This is the hallmark feature of the efficient lung, as the total surface area influences its ability to receive deoxygenated blood and inversely supply the heart with oxygen during respiration. Any disease which results in destruction to the alveoli will ultimately reduce the surface area available for gas exchange and in turn result in a reduction of pulmonary function and quality of life for the individual.

## 1.3 Chronic Obstructive Pulmonary Disease

Having classically been defined as consisting of two distinct, but intertwined, phenotypes COPD is a progressive disease leading to airflow limitations and reduced quality of life. A patient with chronic bronchitis, often referred to as a “blue bloater”, can be visualized as a person with a larger stocky build and a history of a chronic cough.<sup>4</sup> A patient with emphysema, often referred to as a “pink puffer”, will be someone with recent weight loss and abnormal physical weakness.<sup>4</sup> The current diagnostic criteria for COPD are outlined by the Global Initiative for Chronic Obstructive Lung Disease (GOLD) criteria.<sup>19</sup> The GOLD severity grades are provided in **Table 1-1** where  $FEV_1$  is an airflow measurement taken using a spirometer explained in more detail in **Section 1.5.1**.

**Table 1-1: GOLD Severity Grades**

Patient with $FEV_1/FVC < 70\%$		
GOLD I	Mild	$FEV_1 \geq 80\%_{pred}$
GOLD II	Moderate	$50\% \leq FEV_1 < 80\%_{pred}$
GOLD III	Severe	$30\% \leq FEV_1 < 50\%_{pred}$
GOLD IV	Very Severe	$FEV_1 < 30\%_{pred}$

$FEV_1$  = forced expiratory volume in 1 second; FVC = forced vital capacity

### 1.3.1 Chronic Bronchitis

Chronic bronchitis is inflammation of the bronchial tubes, primarily in the mucus glands.<sup>4</sup> This inflammation results in an over-production of mucus by the goblet cells which are located on the epithelial lining of the respiratory tracts.<sup>20</sup> The combination of mucus lining the bronchial tubes and the inflammation results in airflow limitations. The primary cause of chronic bronchitis is cigarette smoking, but that is not the only cause.<sup>4,21</sup>

### 1.3.2 Emphysema

Emphysema affects the airspace distal to the terminal bronchioles. It is characterized by the destruction of the walls of the alveolar ducts, sacs, or both.<sup>4</sup> It is a result of an imbalance of proteases due to either an increased production of proteases or reduced production of antiproteases.<sup>22</sup> There are two main types of recognized emphysema (**Figure 1-2**): Centriacinar emphysema, where destruction is limited to the central lobule leaving the alveolar ducts and sacs unharmed and panacinar emphysema where destruction occurs across the entire lobule.

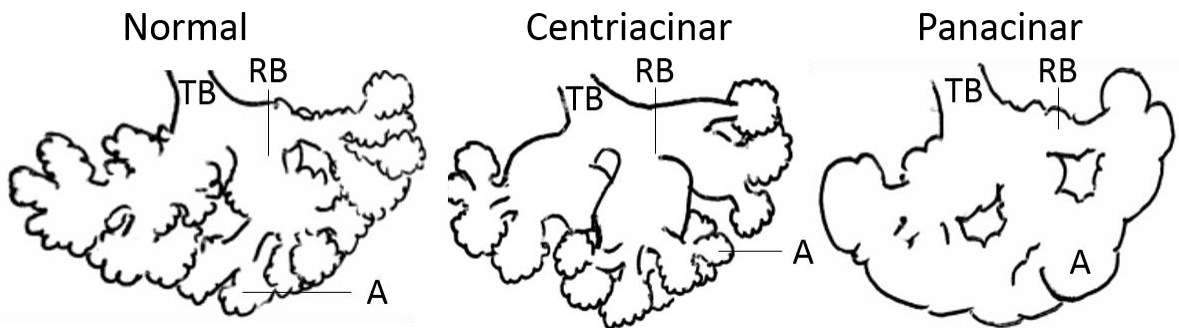


**Figure 1-2: Centriacinar and Panacinar Emphysema**

Normal respiratory bronchioles, respiratory bronchioles affected by centriacinar emphysema where the emphysema is confined the terminal and respiratory bronchioles (TB and RB). This destruction is extended to the alveoli (A) in panacinar emphysema. Adapted from West, JB, Pulmonary Pathophysiology: The Essentials, 4<sup>th</sup> Edition.<sup>4</sup>

The destruction of the lung parenchyma can be seen in **Figure 1-3** showing micro-CT images of a healthy young subject, healthy elderly subject and an ex-smoker. All three images have the same field of view (FOV) = 40mm.

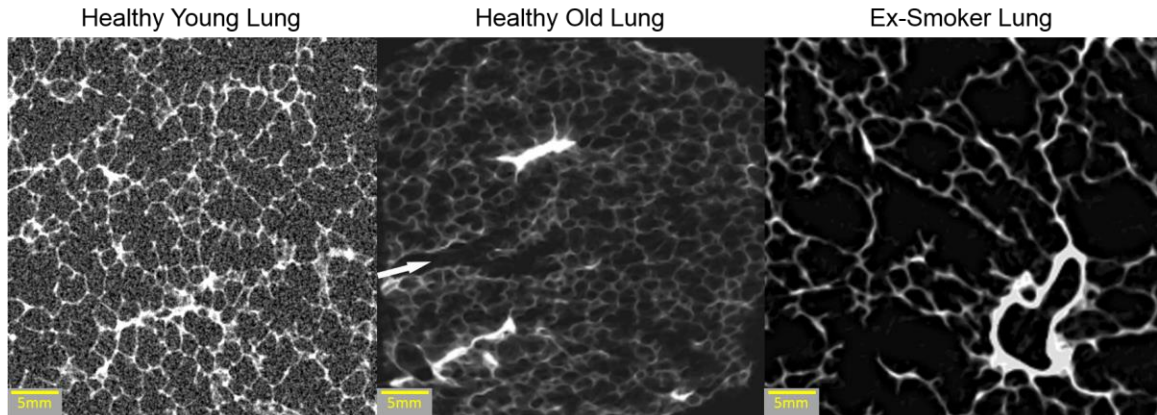


**Figure 1-3: Micro-CT Lung Images**

Micro-CT images showing a healthy young lung with tightly packed alveoli, a healthy old lung<sup>23</sup> showing gradual enlargement of the lung parenchyma and an ex-smoker lung<sup>23</sup> showing emphysematous destruction of the lung parenchyma. (Healthy young lung courtesy of Dr. Vasilescu and Dr. Hogg (UBC)). Healthy Old Lung and Ex-Smoker Lung reproduced with permission (**Appendix A**).

Emphysema is most frequently encountered in the proximal respiratory bronchioles in the upper lobes.<sup>24,25</sup> This is referred to as centrilobular emphysema and is primarily associated with smoking related emphysema. Emphysema can also be located distal to the respiratory bronchioles localized in the basal portion of the lung. This pattern of emphysema is referred to as panlobular emphysema and is characteristic of, but not limited to, AATD related emphysema.<sup>26</sup>

## 1.4 Alpha-1 Antitrypsin Deficiency

### 1.4.1 Biology

AATD was first described in 1963 by Laurell and Eriksson.<sup>27</sup> AATD is an underdiagnosed genetic condition affecting up to 1 in 1500 people of European descent.<sup>6,28</sup> It causes mutations in the SERPINA1 gene which contains instructions for producing a protein called alpha-1 antitrypsin. This protein protects the body from neutrophil elastase, which is released from white blood cells in response to infection but will attack healthy tissue if not regulated.<sup>29,30</sup> The normal allele of the SERPINA1 gene, M, results in normal levels of alpha-1 antitrypsin. Two other variants the S and Z variants produce decreasing amounts of alpha-1 antitrypsin.<sup>31</sup> There are over 100 different alleles worldwide.<sup>32</sup>

### 1.4.2 Liver Disease

Approximately 15% of all alpha-1 antitrypsin deficiency sufferers will develop liver disease.<sup>33</sup> As the alpha-1 antitrypsin is not secreted properly<sup>34</sup> (as a result of protein misfolding) it accumulates in the liver and can cause liver cirrhosis, an accumulation of liver scar tissue.<sup>35</sup>

### 1.4.3 Lung Disease

AATD primarily manifests in the form of panlobular emphysema. The imbalance of neutrophil elastase will result in destruction of connective tissue within the lungs and a breakdown of the alveoli leading to reduced surface area and in turn diminishing the lungs' capacity for gas exchange. Emphysema as a result of AATD predominately affects the basal portion (~64% of patients)<sup>36</sup> of the lung due to the gravitational dependence of pulmonary blood flow. This is not always the case and upper lobular emphysema can also occur as can other respiratory disorders such as bronchiectasis.<sup>37</sup>

### 1.4.4 Augmentation Therapy

At this time there is no cure for AATD and current treatment is geared solely towards symptomatic relief.<sup>32</sup> Intravenous supplementation of exogenous alpha-1 antitrypsin has been shown to both slow the decline of the forced expiratory volume in 1 second (FEV<sub>1</sub>) in patients with AATD<sup>38,39</sup> and slow the decline in lung tissue density as measured by x-ray computed tomography.<sup>7</sup> Augmentation therapy is a costly procedure and there are some debates on who would benefit the most from treatment.<sup>40</sup> In addition, recent clinical trials have not shown significant changes in exercise capacity, patient perceived quality of life, exacerbations or hospitalizations as a result of treatment.<sup>7</sup> To overcome this, there is preliminary work examining novel treatments for AATD emphysema including gene therapy<sup>41-44</sup> and pluripotent stem cells.<sup>45,46</sup> In order to accurately gauge the efficacy of these novel treatments, pulmonary imaging must be employed as it has previously played an important role in demonstrating treatment efficacy with respect to lung density changes. However, to truly measure airspace enlargement *in vivo* lung morphometry techniques, which can give measures of airspace enlargement and surface-to-volume ratios, are required. These measurements must be sufficiently sensitive to detect small changes in

early and mild disease as well as severe end stage emphysema. If a sensitive measurement of disease and airspace enlargement were developed and applied to clinical efficacy evaluation of novel treatments it would be possible to perform smaller single-centre studies. This would result in a drastic reduction in costs and ultimately aid in the development of novel treatments of AATD emphysema.

## 1.5 Clinical Measurements of Lung Disease

### 1.5.1 Spirometry

Worldwide, spirometry provides the gold standard measurement for the diagnosis and clinical evaluation of COPD.<sup>19</sup> Spirometry tests by patients who are coached by a trained pulmonary technologist for which there are accepted guidelines on reproducibility and evaluation.<sup>47</sup> Spirometry measurements are inexpensive and reproducible while requiring little specialized equipment or training; however, they rely solely on airflow measurements taken at the mouth and therefore provide a single global measurement representing lung function.<sup>47</sup> This unfortunately fails to unmask the many faces of COPD and hides its underlying heterogeneity.<sup>48,49</sup> The primary measurement of airflow limitation is the FEV<sub>1</sub> which is a measurement of the maximum amount of air exhaled during the first 1 second of a forced expiration. **Figure 1-4** shows a sample flow volume curve for a normal healthy individual (**Figure 1-4A**) and a flow volume curve for someone with an obstructive lung disease (**Figure 1-4B**). The total volume of air exhaled during this breathing maneuver is the forced vital capacity (FVC).

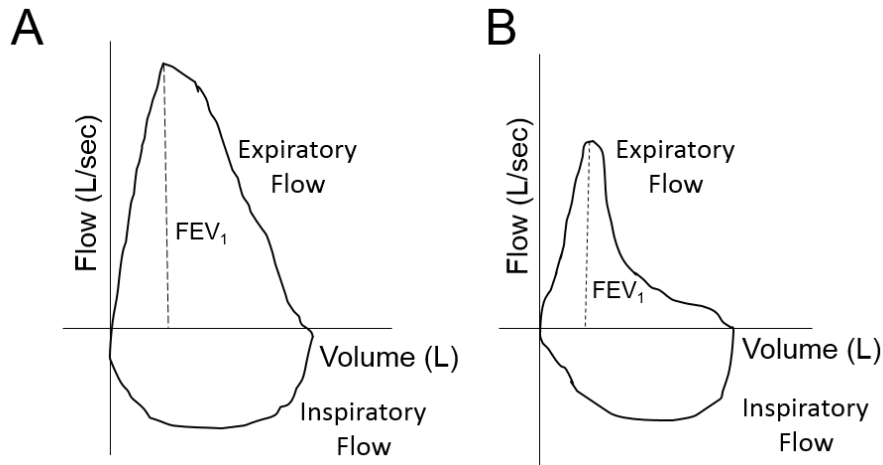


**Figure 1-4: Flow Volume Curve**

Sample flow volume curves for a healthy (A) patient and someone with obstructive lung disease (B). In obstructive lung disease, flow rates are slower resulting in a lower FEV<sub>1</sub>.

### 1.5.2 Lung Volumes and Capacities

In addition to FEV<sub>1</sub> and FVC it is possible to measure patient lung volumes using a plethysmograph. Briefly, a plethysmograph is a closed system in which the patient sits that is used to measure lung volumes, specifically the functional residual capacity (FRC), total lung capacity (TLC) and the residual volume (RV). FRC is the volume of air in the lungs remaining at the end of a passive expiration during a normal breathing cycle and RV is the volume of air in the lungs remaining at the end of a full expiration. To accomplish this Boyles law is implemented and using measured pressure differences one can derive the aforementioned lung volumes.<sup>50</sup>

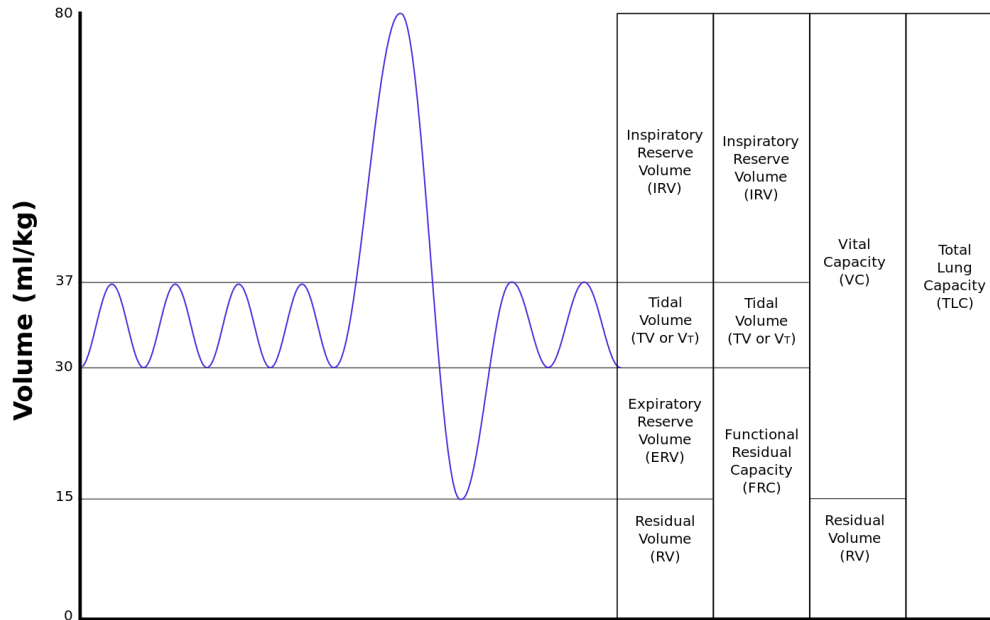


**Figure 1-5: Lung Volumes**

A volume time curve showing clinically relevant lung volumes. Relevant lung volumes for this work are: **Residual Volume (RV)**, the volume remaining after full expiration; **Functional Residual Capacity (FRC)**, the volume remaining after passive expiration and **Total Lung Capacity (TLC)**; the total lung volume after a full inspiration.

The measurement of TLC and RV/TLC is important as it represents hyperinflation of the lungs which is a hallmark sign of COPD due to either the loss of the elastic property of the lung parenchyma or an obstruction in the passage of air.

### 1.5.3 Diffusing Capacity of the Lung for Carbon Monoxide

The diffusing capacity of the lung for carbon monoxide ( $DL_{CO}$ ) test measures the amount of oxygen passing from the alveolar sacs into the blood. During the test the patient breathes in a test gas containing a small amount of tracer gas (CO) and holds their breath.<sup>51</sup> CO is used due to its affinity to bind to hemoglobin, making the uptake of CO diffusion limited as opposed to perfusion limited. This means that the amount of gas taken up is solely dependent on diffusion and not the amount of available blood flow.<sup>4</sup> Upon a breath-hold of 10 seconds the patient exhales and the exhaled gas is tested to determine the amount of tracer gas that was absorbed during the duration of the breath hold.<sup>51</sup> This test is especially important in patients with emphysema as the destruction of the alveolar sacs leads to a decreased capacity for gas exchange between the air sacs and blood. A measurement of  $DL_{CO}$  normalized to the alveolar volume ( $DL_{CO}/VA$ ) has been proposed as a more specific



measurement.<sup>52,53</sup> Although simple and quick, this tests lacks reproducibility over time<sup>54</sup> and therefore may be unattractive in cases where longitudinal monitoring may be required. A low DL<sub>CO</sub> combined with an increase in TLC, RV/TLC is a classic sign of emphysema as observed by pulmonary function testing.<sup>55</sup>

#### 1.5.4 Six-Minute Walk Test

Patient exercise capacity can be measured by performing the six-minute walk test (6MWT). In the 6MWT the patient walks at a self-set pace, resting as necessary, on a flat surface for six minutes. The six minute walk test does not provide specific information of the limiting exercise factor but is reflective of the activities performed during day to day life. Before and after performing the six minute walk test the patient answers two questions on perceived levels of exhaustion<sup>56</sup> and has measurements of arterial oxygenation (S<sub>P</sub>O<sub>2</sub>) and heart rate taken. All six minute walk tests performed for this thesis are to American Thoracic Society guidelines.<sup>57,58</sup>

#### 1.5.5 St. George's Respiratory Questionnaire

The St. George's Respiratory Questionnaire (SGRQ)<sup>59</sup> is designed to measure the overall impact that respiratory disease has on the quality of life as perceived by the patient. There are two sections a symptoms section and an activities section which relate to the symptoms experienced and the burden of the disease. The questionnaire is scored from 0 to 100 with higher scores indicating worse perceived quality of life and symptoms.

### 1.6 X-Ray Computed Tomography

#### 1.6.1 Theory

At its most basic level, x-ray computed tomography (CT) is an extension of planar x-ray imaging to three dimensions using a rotating x-ray tube and detector combined with a motorized patient bed.<sup>60</sup> The contrast in the image is related to the radiodensity of the scanned material where each value represents a Hounsfield unit (HU) corresponding to:

$$HU = 1000 * \frac{\mu - \mu_{water}}{\mu_{water} - \mu_{air}} \quad (1-1)$$

With  $\mu$  being the linear attenuation coefficient and 0 HU being defined as the radiodensity of distilled water at standard pressure and temperature.

### 1.6.2 Pulmonary X-Ray Computed Tomography

CT imaging of the lung can be used to visualize regions of low attenuation and quantify both gas trapping and emphysema. Typical lung parenchyma attenuation values are between -910 and -500 HU.<sup>61</sup> A CT scan performed at full expiration can be used to quantify regions of gas trapping which are regions where gas is not cleared through exhalation. To do so the regions of the lung  $<-856$  HU are examined.<sup>62</sup> A full inspiration CT can be used to quantify regions of emphysema. Using the attenuation  $<-950$  HU as an emphysema threshold.<sup>63</sup> This can be quantified using the relative area of the CT density histogram with values  $<-950$  HU ( $RA_{950}$ ).  $RA_{950}$  measurements correlate well with radiologist scores,<sup>64</sup> histology<sup>65</sup> and pulmonary function testing.<sup>66</sup> Regions of the CT lung density histogram representing airspace enlargement are shown in **Figure 1-6** for a healthy never-smoker and representative AATD subject. Combining inspiration and expiration CT scans together, a regional map of gas trapping and emphysema can be made.<sup>67</sup> This method, called parametric response mapping, co-registers the inspiratory and expiratory CT scans and generates a lung map showing regions of gas trapping and emphysema. These methods can provide regional information of emphysema and gas trapping throughout the lung. In addition to quantifying regions of emphysema and gas trapping CT provides a measurement of lung density (g/L).<sup>68,69</sup> Unfortunately, current spatial resolutions available with CT are not fine enough to visualize the smaller airways. There are other quantification methods such as examining low attenuating clusters (LAC)<sup>70</sup> where the cumulative size distribution of these low attenuating clusters ( $<-950$  HU) are described by a power law relationship with the number of low attenuating clusters. This in principle relates the size of these emphysematous lesions and the number of lesions using CT. This can be graphically illustrated as low attenuating spheres where the size of the sphere is proportional to the cumulative lesion size.

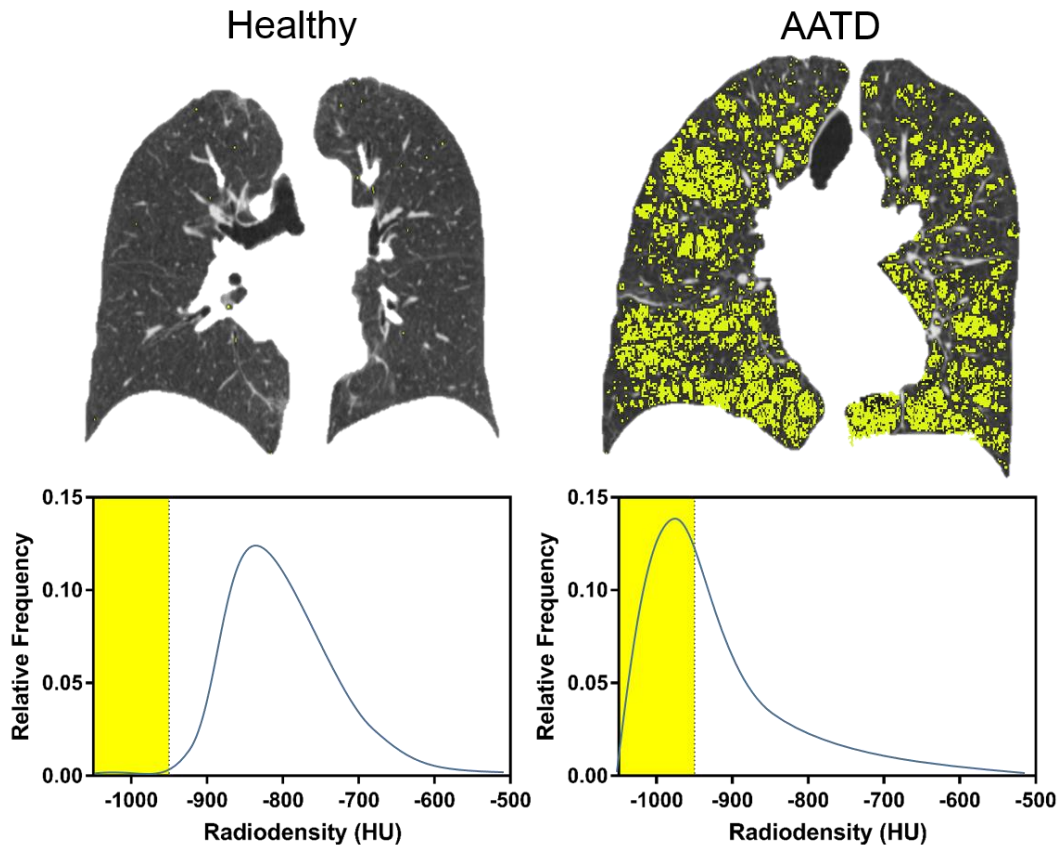


**Figure 1-6: CT Radiodensity and Histogram**

CT images with yellow masks corresponding to voxels <-950 HU and the corresponding whole lung CT radiodensity histogram for a healthy never-smoker and subject with AATD

Since the development of micro-CT spatial resolutions approaching 4  $\mu\text{m}$  may be obtained.<sup>71</sup> Micro-CT as a method of visualizing and quantifying lung morphometry has been thoroughly demonstrated in mice,<sup>72</sup> pigs<sup>73</sup> and cadaveric human lung specimens,<sup>23,71</sup> including AATD donor lungs;<sup>74</sup> however, the scan speed and radiation exposure required to execute a scan leaves the feasibility of micro-CT geared solely to *ex-vivo* imaging.<sup>75,76</sup>

## 1.7 Magnetic Resonance Imaging

### 1.7.1 Theory

Conventional  $^1\text{H}$  MRI of the body is possible due to the high concentration of  $^1\text{H}$  molecules comprising various biological tissues. The gyromagnetic ratio ( $\gamma$ ) of a nucleus will in part determine the MR signal. The high  $\gamma$  of  $^1\text{H}$  ( $\gamma_{^1\text{H}} = 42.6 \text{ MHz T}^{-1}$ ) combined with the natural abundance of  $^1\text{H}$  located inside biological tissue provides ample signal for imaging most

of the body. Unfortunately, the lungs have incredibly low density (133g/L - 200g/L)<sup>77</sup> and have millions of air tissue interfaces which result in magnetic field inhomogeneities within the lung parenchyma. This makes clinically available <sup>1</sup>H MRI unsuitable for quantitative evaluation of the lung or the diseases which affect it.

### 1.7.2 Pulmonary Magnetic Resonance Imaging

Conventional <sup>1</sup>H MRI of the lungs is difficult due to the high concentration of air contained within the lungs, and consequently the low tissue density.<sup>77</sup> This is made further complicated by the large number of air-tissue interfaces which affect magnetic field homogeneity within the lungs. For these reasons, the lungs appear as dark voids (**Figure 1-7**) providing little to no information on lung structure-function.

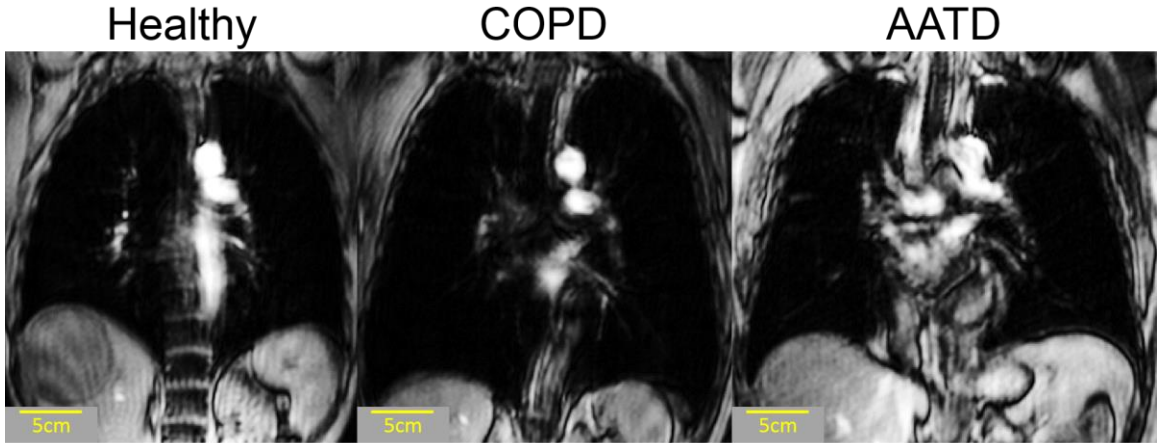


**Figure 1-7: <sup>1</sup>H Thorax image for representative NS, COPD and AATD Subjects**

This limitation can be circumvented by using multinuclear MRI and as opposed to measuring <sup>1</sup>H density, one measures the relative density of an inhaled hyperpolarized noble-gas. Through spin-exchange optical pumping, noble-gases can be hyperpolarized and used for imaging of the lungs after inhalation.<sup>78</sup> This is important because the MRI signal is proportional, to the following factors:<sup>79</sup>

$$S \propto \frac{1}{2} N |\gamma| \hbar \omega_0 P_N \quad (1-2)$$

Where S is the MRI signal, N is the number of spins,  $\gamma$  is the gyromagnetic ratio,  $\hbar$  is the reduced Plank constant,  $\omega_0$  is the Larmor frequency and  $P_N$  is the nuclear polarization. In

the case of  $^1\text{H}$  MRI the high  $N$  provides adequate signal for imaging purposes; however, in the case of hyperpolarized noble-gas imaging thermally polarized noble-gas to provides inadequate signal due to the small  $N$  and  $P_N$ . However, this can be overcome by raising the  $P_N$  through external polarization of the noble-gas. This technique allows visualization of gas dispersion within the lungs.

### 1.7.2.1 $^1\text{H}$ Methods

There are however methods utilizing traditional  $^1\text{H}$  imaging which provide information suitable for quantitative image analysis. These methods are currently under investigation in research settings but may serve to provide translatable lung imaging. Two methods are Fourier decomposition (FD) MRI<sup>80</sup> and Ultrashort Echo Time (UTE) MRI.<sup>81</sup>

#### 1.7.2.1.1 Fourier Decomposition

During a period of free breathing, multiple images are taken of a single slice through the lungs. The images are then deformably registered<sup>82</sup> to each other to account for cardiac motion and the varying lung volumes throughout the respiratory cycle. The discrete Fourier transform is taken at each lung voxel and ventilation and perfusion maps can be obtained by observing the corresponding peak at either the respiratory rate (ventilation) or cardiac rate (perfusion). Ventilation maps obtained from FD MRI have been shown to correlate with ventilation maps obtained from  $^3\text{He}$ .<sup>83</sup>

#### 1.7.2.1.2 Ultrashort Echo Time

To overcome the difficulties in lung imaging a method using echo times ( $T_E$ ) of  $\sim 50\mu\text{s}$  and 3D radial k-space trajectories has been developed. MRI is performed at four lung volumes: full expiration, FRC, FRC+1L and full inhalation. Absolute signal intensity is normalized to the liver and dynamic proton maps (registered to FRC+1L) can be computed using the lung volumes. The UTE signal has been shown to be related to lung volume suggesting a relationship to tissue density.<sup>84</sup> It is also related to gas-trapping in asthmatics.<sup>85</sup>

## 1.7.2.2 Hyperpolarized Methods

### 1.7.2.2.1 Spin Physics and Polarization

By using spin-exchange optical pumping (SEOP) high levels of  $^3\text{He}$  or  $^{129}\text{Xe}$  polarization can be achieved.<sup>79</sup> The SEOP system uses circularly polarized resonance light which is absorbed by rubidium housed within a glass cell. Contained within the same glass cell is the noble-gas used in the spin-exchange,  $^3\text{He}$  in this case. Angular momentum is transferred through binary collisions from the polarized rubidium to the  $^3\text{He}$ . Over time as collisions increase, this causes an increase of the  $^3\text{He}$  nuclear polarization to several orders of magnitude larger than the thermal polarization obtained using magnetic fields. A full theoretical description of SEOP of noble-gas nuclei can be found in a review by Walker and Happer 1997.<sup>86</sup>

### 1.7.2.2.2 Static Ventilation MRI

By imaging the spin density of the polarized noble-gas during a breath-hold, visualization of gas distribution throughout the lungs can be achieved. These images are coined static ventilation (SV) images and as the name indicates they give a single static image of gas distribution. This is shown in **Figure 1-8**, these are the same subjects and slices as Figure 7. This image, can be qualitatively analyzed by identifying regions of hypo-intense signal (signal voids) as well as regions of hyper-intense signal. These regions can also be quantified using semi-automated segmentation methods,<sup>87</sup> where the  $^1\text{H}$  and  $^3\text{He}$  images are co-registered using an affine transformation, to determine the ventilation defect percent (VDP) which is the volume of ventilation defects (signal voids) normalized to the thoracic cavity volume.

$$VDP [\%] = \frac{\textit{Ventilation defect volume}}{\textit{Thoracic cavity volume}} \times 100\% \quad (1-3)$$

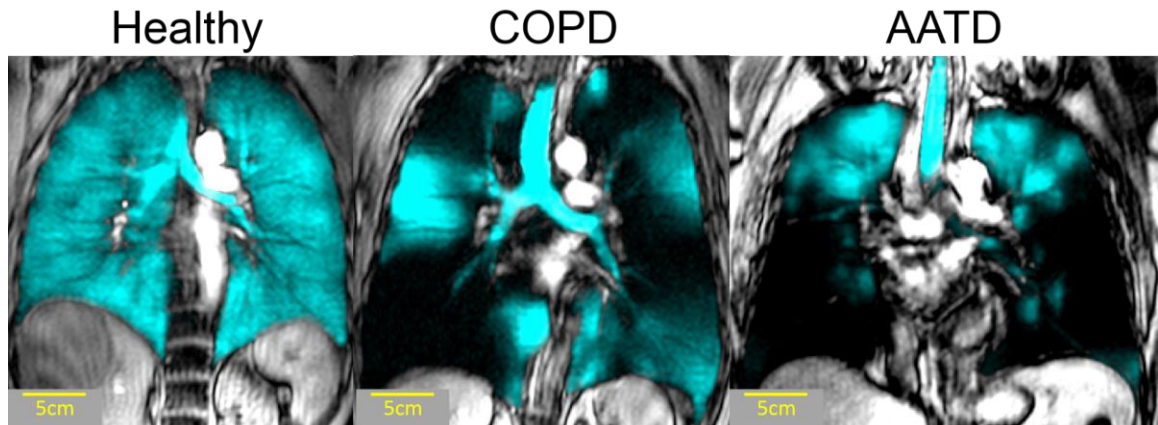


**Figure 1-8: Static ventilation images for representative NS, COPD and AATD subjects**

$^3\text{He}$  static ventilation (cyan) overlaid on  $^1\text{H}$  thorax image for a representative subjects

VDP has been shown to correlate with aging,<sup>88</sup> ventilation homogeneity,<sup>89</sup> and spirometry.<sup>90</sup> VDP shows response to bronchodilation in asthmatics,<sup>91</sup> as well as response to bronchoconstriction (methacholine).<sup>92</sup>

#### 1.7.2.2.3 Diffusion-weighted MRI

Using a similar method to what is used to acquire SV images, and employing a diffusion-weighted pulse sequence<sup>93</sup> (**Figure 1-9**) diffusion-weighted images can be acquired. Due to the loss of the MR signal at high b-values, the highest b-values are acquired first to maximize the signal at those values. The diffusion gradient is shown in blue for interleaves 2-5. These images allow visualization and quantification of the extent to which the noble-gas molecules are able to diffuse within the confining space of the alveolus.<sup>94</sup>

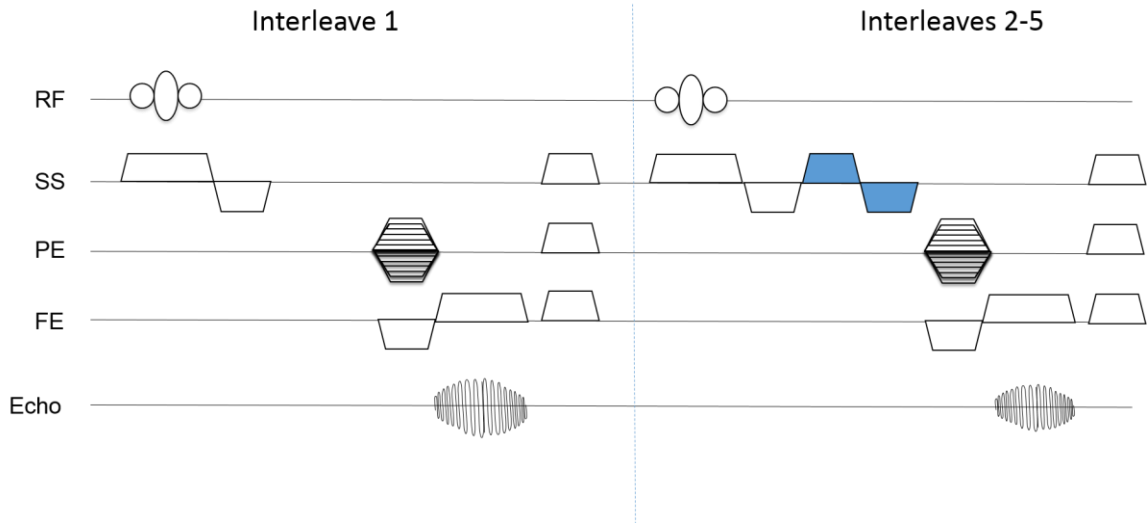


**Figure 1-9: Diffusion-weighted Pulse Sequence**

A multiple b-value fast gradient recalled echo (FGRE) pulse sequence. Interleave 1 acquires a non-diffusion-weighted static ventilation image and interleaves 2-5 acquire diffusion weighted images due to the diffusion gradient (in blue). The size and strength of the diffusion gradient are varied to acquire multiple b-values.

#### 1.7.2.2.4 Apparent Diffusion Coefficient

In a confined medium, such as an airway or alveolus, the root mean square displacement ( $\langle r^2 \rangle$ ) of a noble-gas molecule and its diffusion time (t) can be related to an apparent diffusion coefficient (ADC) giving a relative measure of confinement:

$$ADC = \frac{\langle r^2 \rangle}{2t} \quad (1-4)$$

Diffusion-weighted MRI can extract this ADC through diffusion-weighted pulse sequences (**Figure 1-9**). First, a non-diffusion-weighted (static ventilation) image is acquired as described in **Section 1.7.2.2.2**, and for the same slice a second, diffusion-weighted, image is acquired. For this image, the so-called b-value [ $\frac{s}{cm^2}$ ] indicates the size and strength of this diffusion gradient (**Figure 1-10**).



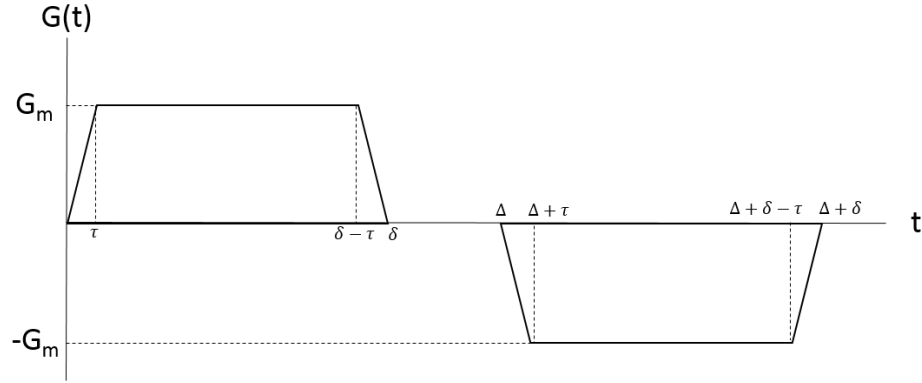


**Figure 1-10: Diffusion sensitizing pulse gradient waveform**

A bipolar trapezoidal diffusion sensitizing gradient.  $G_m$  = maximum gradient amplitude,  $\tau$  = gradient ramp up/down time,  $\delta$  = lobe duration,  $\Delta$  = diffusion time.

$$b = (\gamma G_m)^2 \left[ \delta^2 \left( \Delta - \frac{\delta}{3} \right) + \tau \left( \delta^2 - 2\Delta\delta + \Delta\tau - \frac{7}{6}\delta\tau + \frac{8}{15}\tau^2 \right) \right] \quad (1-5)$$

With  $\gamma$  = gyromagnetic ratio,  $G_m$  = maximum gradient,  $\tau$  = gradient ramp up/down time,  $\delta$  = lobe duration and  $\Delta$  = diffusion time. The b-value is chosen based on the confining medium and the free diffusion of the noble-gas used. A good rule of thumb for b-value selection is  $(b \cdot ADC) \cong 1$ .<sup>95</sup> This bipolar diffusion gradient works by dephasing the nuclear spins,<sup>93</sup> this effectively encodes the initial position of the nuclei. The negative portion of the gradient will rephase the spins but it will not completely rephase them as diffusion has occurred. Thus, by relating the relative signal intensities in both the diffusion-weighted and non-diffusion-weighted images the ADC can be measured as shown in equation 1-7:

$$\frac{S(b)}{S_0} = \exp(-b \cdot ADC) \quad (1-6)$$

$$ADC(b) = \frac{\ln\left(\frac{S_0}{S(b)}\right)}{b} \quad (1-7)$$

Where commonly used b-values for lung imaging range between 1.6 and 6.4 s/cm<sup>2</sup> for <sup>3</sup>He and 12 and 30 s/cm<sup>2</sup> for <sup>129</sup>Xe. **Figure 1-11** shows diffusion and non-diffusion-weighted <sup>3</sup>He ventilation images for the same slice in a subject with AATD.

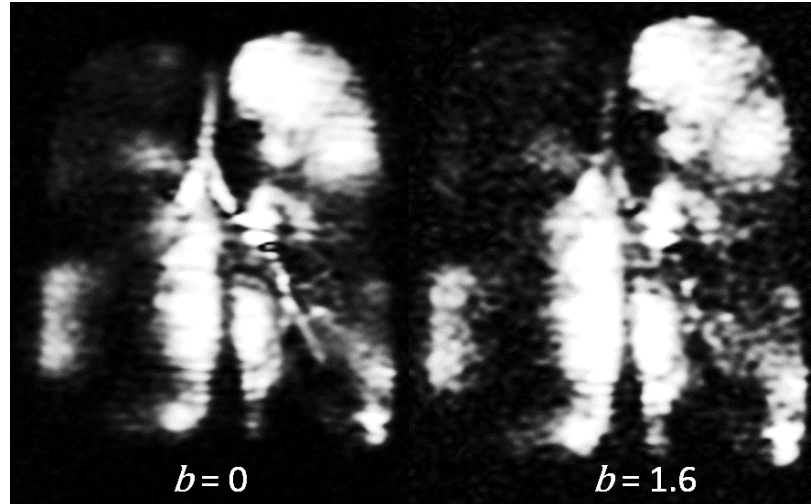


**Figure 1-11: Non-Diffusion and Diffusion-weighted  $^3\text{He}$  Ventilation Image**

When **Equation 1-7** is applied to each voxel, a map of ADC can be generated. **Figure 1-12**, shows the ADC map generated from the images in **Figure 1-11**.

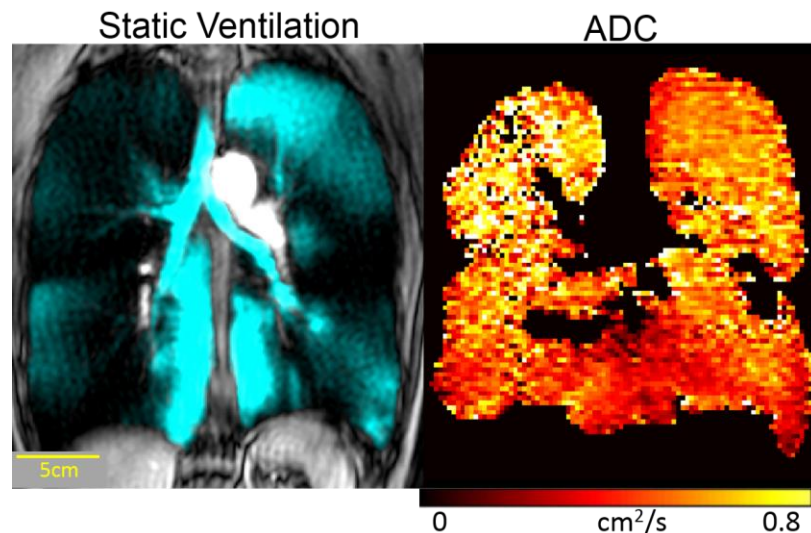


**Figure 1-12: Static ventilation and ADC for AATD subject**

Static ventilation and slice matched ADC image for a representative AATD subject. Female, 58 years old.  $\text{FEV}_1 = 32\%_{\text{pred}}$ ,  $\text{FEV}_1/\text{FVC} = 31\%$ ,  $\text{RV}/\text{TLC} = 62\%$ ,  $\text{DLCO} = 53\%_{\text{pred}}$ ,  $\text{ADC} = 0.43 \text{ cm}^2/\text{s}$ .

$^3\text{He}$  ADC has been shown to correlate well with patient measurements of disease,<sup>94</sup> histological measurements of  $L_m$ <sup>96</sup> and CT measurements of emphysema.<sup>97</sup> It is elevated in asthmatics post methacholine challenge, representing gas trapping.<sup>92</sup> ADC is also related to lung inflation levels<sup>98</sup> as well as patient age.<sup>99,100</sup> There has been a large body of work

performed using  $^3\text{He}$ , there have been preliminary reports of  $^{129}\text{Xe}$  ADC in healthy volunteers and subjects with COPD<sup>101-103</sup> with  $^{129}\text{Xe}$  ADC measurements correlating with histological measurements.<sup>104</sup>

#### 1.7.2.2.5 Multiple b-value ADC Magnetic Resonance Imaging

By varying the b-values used, a set of multiple b-value images can be acquired for the same slice. During an acquisition a molecule will either experience free unrestricted diffusion, or it will experience restricted diffusion due to the presence of airspace walls. At different b-values varying number of molecules will experience restriction due to the presence of the airspace walls. This technique can be used to probe varying length scales. Using the signal decay as a function of b-value measures a voxel-wise mean of airspace sizes. This technique provides a more sensitive measurement, as compared to two b-value ADC measurements, of alveolar size

#### 1.7.2.3 Measurements of Alveolar Geometry using Multiple-b ADC

Measurements of alveolar geometry can be made using assumptions of the noble gas displacement within the alveolus. The assumption made in this thesis, based on previous work, is that the diffusion within the airways is anisotropic. A cylindrical geometry of the alveoli and alveoli ducts is assumed.

##### 1.7.2.3.1 Weibel Model of Alveolar Geometry

The primary geometrical representation of the acinar airways is the Weibel representation.<sup>18</sup> In this representation (**Figure 1-13**), the airway is approximated as an

infinite cylinder (**Figure 1-14**) with inner and outer radii ( $r$  and  $R$ , respectively) and 8 alveoli surrounding the cylinder with height  $h=R-r$ .

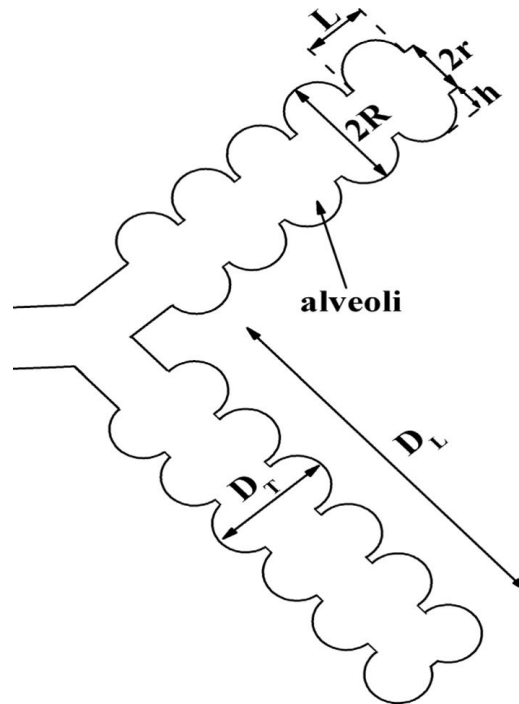


**Figure 1-13: Weibel representation of the acinar duct**

An acinar duct covered in a sleeve of alveoli.  $R$  = external airway radius,  $r$  = internal airway radius,  $L$  = alveoli length,  $h$  = alveoli sheath,  $D_L$  = MRI longitudinal diffusion coefficient,  $D_T$  = MRI transverse diffusion coefficient

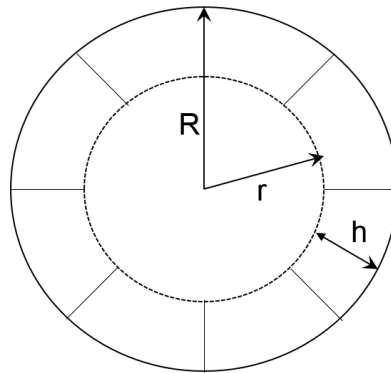


**Figure 1-14: Infinite cylinder geometry**

The Weibel representation is considered as a cylindrical tube surrounded by a sleeve of alveoli.  $R$ = external airway radius,  $r$  = internal airway radius.

The outer cylinder represents a sleeve of alveoli surrounding the alveolar duct. The diffusion of the noble gas within the acinar airways is assumed to be anisotropic, consisting

of both longitudinal ( $D_L$ ) and transverse ( $D_T$ ) diffusion coefficients. The total MR signal acquired from a single voxel is:<sup>105</sup>

$$S(b) = S_0 \exp(-bD_T) \left( \frac{\pi}{4b(D_L - D_T)} \right)^{\frac{1}{2}} \Phi \left[ (b(D_L - D_T))^{\frac{1}{2}} \right] \quad (1-8)$$

Where  $\Phi$  is the error function ( $\Phi(x) = \frac{1}{\sqrt{\pi}} \int_{-x}^x e^{-t^2} dt$ ). Using this MR signal as well as Monte-Carlo derived equations<sup>105</sup> for the transverse and longitudinal diffusion are used to find geometrical expressions for the inner ( $r$ ) and outer radii ( $R$ ). These geometrical values can then be used to find the alveolar length, surface-to-volume ratio and mean linear intercept as follows:

$$L = 2R \sin\left(\frac{\pi}{8}\right) \quad (1-9)$$

$$\frac{S}{V} = \frac{2\pi RL + 2\pi(R^2 - r^2) + 16(R - r)L}{\pi R^2 L} \quad (1-10)$$

$$L_m = 4 \frac{V}{S} \quad (1-11)$$

Measurements of airspace size ( $L_m$ ) measured using this geometrical model have been shown to correlate with histology,<sup>106</sup> show differences between elderly smokers and never-smokers<sup>107,108</sup> as well as correlate with disease severity.

## 1.8 Thesis Objectives

In this thesis, my objective was to evaluate multiple b-value MRI in subjects with AATD and examine regional MRI biomarkers of emphysema. This is important because in AATD disease manifests at a young age and longitudinal evaluation is important both clinically and in the process of development of novel treatments. I hypothesized that subjects with a clinical diagnosis of AATD would show significantly elevated morphometry values as compared to ex-smokers with COPD and age-matched healthy elderly never-smokers. I would expect to observe these differences since in AATD disease begins from birth and as such, would differ from smoking-related disease and that observed in senile emphysema.

To test this hypothesis, I performed a proof-of-concept demonstration in a small group of subjects with AATD, subjects with smoking related emphysema and a group of healthy age-matched never-smokers. I compared whole lung diffusion weighted measurements of airspace enlargement across all three groups and examined these measurements regionally throughout the lung. These measurements were also compared to standard clinical measurements such as spirometry and CT.

## 1.9 References

- (1) Kac, M. Can one hear the shape of a drum? *The american mathematical monthly* 1966; 73: 1-23.
- (2) Global Alliance against Chronic Respiratory Diseases. World Health Organization Fact Sheet N 315, <<http://www.who.int/mediacentre/factsheets/fs315/en/>> (2012)
- (3) Chapman, K., Bourbeau, J. & Rance, L. The burden of COPD in Canada: results from the Confronting COPD survey. *Respiratory Medicine* 2003; 97: S23-S31.
- (4) West, J. B. *Pulmonary pathophysiology: the essentials*. (Lippincott Williams & Wilkins, 2011).
- (5) Eriksson, S. Pulmonary emphysema and alpha1-antitrypsin deficiency. *Acta Medica Scandinavica* 1964; 175: 197-205.
- (6) Stoller, J. K. & Aboussouan, L. S.  $\alpha$ 1-antitrypsin deficiency. *The Lancet* 2005; 365: 2225-2236.
- (7) Chapman, K. R. *et al.* Intravenous augmentation treatment and lung density in severe  $\alpha$ 1 antitrypsin deficiency (RAPID): a randomised, double-blind, placebo-controlled trial. *The Lancet* 2015.
- (8) Hsia, C. C., Hyde, D. M., Ochs, M. & Weibel, E. R. An official research policy statement of the American Thoracic Society/European Respiratory Society: standards for quantitative assessment of lung structure. *American journal of respiratory and critical care medicine* 2010; 181: 394-418.
- (9) Ochs, M. A brief update on lung stereology. *Journal of microscopy* 2006; 222: 188-200.
- (10) Ochs, M. & Mühlfeld, C. Quantitative microscopy of the lung: a problem-based approach. Part 1: basic principles of lung stereology. *American Journal of Physiology-Lung Cellular and Molecular Physiology* 2013; 305: L15-L22.
- (11) Stavngaard, T., Sogaard, L. V., Batz, M., Schreiber, L. & Dirksen, A. Progression of emphysema evaluated by MRI using hyperpolarized 3he (hp 3he) measurements in patients with alpha-1-antitrypsin (a1at) deficiency compared with CT and lung function tests. *Acta Radiologica* 2009; 50: 1019-1026.
- (12) Van Beek, E. *et al.* Hyperpolarised 3He MRI versus HRCT in COPD and normal volunteers: PHIL trial. *European Respiratory Journal* 2009; 34: 1311-1321.
- (13) Diaz, S. *et al.* Progression of Emphysema in a 12-month Hyperpolarized 3 He-MRI Study: Lacunarity Analysis Provided a More Sensitive Measure than Standard ADC Analysis1. *Academic radiology* 2009; 16: 700-707.

- (14) Diaz, S. *et al.* Hyperpolarized <sup>3</sup>He apparent diffusion coefficient MRI of the lung: reproducibility and volume dependency in healthy volunteers and patients with emphysema. *Journal of Magnetic Resonance Imaging* 2008; 27: 763-770.
- (15) Ouriadov, A., Lessard, E., Sheikh, K. & Parraga, G. Pulmonary MRI morphometry modeling of airspace enlargement in chronic obstructive pulmonary disease and alpha-1 antitrypsin deficiency. *Magnetic Resonance in Medicine* 2017.
- (16) West, J. B. *Respiratory physiology: the essentials.* (Lippincott Williams & Wilkins, 2012).
- (17) Ochs, M. *et al.* The number of alveoli in the human lung. *American journal of respiratory and critical care medicine* 2004; 169: 120-124.
- (18) Weibel, E. in *Morphometry of the Human Lung* Ch. 10, 110-135 (Springer Berlin Heidelberg, 1963).
- (19) Vestbo, J. *et al.* Global strategy for the diagnosis, management, and prevention of chronic obstructive pulmonary disease: GOLD executive summary. *American journal of respiratory and critical care medicine* 2013; 187: 347-365.
- (20) Rogers, D. F. The airway goblet cell. *The international journal of biochemistry & cell biology* 2003; 35: 1-6.
- (21) Reid, D. Air pollution as a cause of chronic bronchitis. *Proceedings of the Royal Society of Medicine* 1964; 57: 965.
- (22) MacNee, W. ABC of chronic obstructive pulmonary disease: pathology, pathogenesis, and pathophysiology. *BMJ: British Medical Journal* 2006; 332: 1202.
- (23) Watz, H., Breithecker, A., Rau, W. S. & Kriete, A. Micro-CT of the Human Lung: Imaging of Alveoli and Virtual Endoscopy of an Alveolar Duct in a Normal Lung and in a Lung with Centrilobular Emphysema—Initial Observations 1. *Radiology* 2005; 236: 1053-1058.
- (24) Satoh, K. *et al.* CT assessment of subtypes of pulmonary emphysema in smokers. *CHEST Journal* 2001; 120: 725-729.
- (25) Stavngaard, T., Shaker, S., Bach, K., Stoel, B. & Dirksen, A. Quantitative assessment of regional emphysema distribution in patients with chronic obstructive pulmonary disease (COPD). *Acta Radiologica* 2006; 47: 914-921.
- (26) Kim, W. *et al.* Centrilobular and panlobular emphysema in smokers. *Am Rev Respir Dis* 1991; 144: 1385-1390.



- (27) Laurell, C.-B. & Eriksson, S. The electrophoretic  $\alpha_1$ -globulin pattern of serum in  $\alpha_1$ -antitrypsin deficiency. *Scandinavian journal of clinical and laboratory investigation* 1963; 15: 132-140.
- (28) Pagon, R. A. *et al.* Alpha-1 Antitrypsin Deficiency. 2014.
- (29) Doring, G. The role of neutrophil elastase in chronic inflammation. *American journal of respiratory and critical care medicine* 1994; 150: S114.
- (30) Chua, F. & Laurent, G. J. Neutrophil elastase: mediator of extracellular matrix destruction and accumulation. *Proceedings of the American Thoracic Society* 2006; 3: 424-427.
- (31) Stoller, J. K. & Aboussouan, L. S. A review of  $\alpha_1$ -antitrypsin deficiency. *American journal of respiratory and critical care medicine* 2012; 185: 246-259.
- (32) Köhnlein, T. & Welte, T. Alpha-1 antitrypsin deficiency: pathogenesis, clinical presentation, diagnosis, and treatment. *The American journal of medicine* 2008; 121: 3-9.
- (33) Larsson, C. Natural history and life expectancy in severe alpha1-antitrypsin deficiency, Pi Z. *Acta medica scandinavica* 1978; 204: 345-351.
- (34) Lomas, D. A., Evans, D. L., Finch, J. T. & Carrell, R. W. The mechanism of Z alpha 1-antitrypsin accumulation in the liver. *Nature* 1992; 357: 605-607.
- (35) Fairbanks, K. D. & Tavill, A. S. Liver disease in alpha 1-antitrypsin deficiency: a review. *The American journal of gastroenterology* 2008; 103: 2136-2141.
- (36) Parr, D. G., Stoel, B. C., Stolk, J. & Stockley, R. A. Pattern of emphysema distribution in  $\alpha_1$ -antitrypsin deficiency influences lung function impairment. *American journal of respiratory and critical care medicine* 2004; 170: 1172-1178.
- (37) King, M. A. *et al.* Alpha 1-antitrypsin deficiency: evaluation of bronchiectasis with CT. *Radiology* 1996; 199: 137-141.
- (38) Chapman, K., Stockley, R., Dawkins, C., Wilkes, M. & Navickis, R. Augmentation therapy for alpha 1- antitrypsin deficiency: a meta-analysis of randomized and non-randomized clinical studies. *Eur Respir J* 2005; 26: 288s.
- (39) Chapman, K. R., Stockley, R. A., Dawkins, C., Wilkes, M. M. & Navickis, R. J. Augmentation therapy for  $\alpha_1$  antitrypsin deficiency: A meta-analysis. *COPD: Journal of Chronic Obstructive Pulmonary Disease* 2009; 6: 177-184.
- (40) Sandhaus, R. A. *et al.* The Diagnosis and Management of Alpha-1 Antitrypsin Deficiency in the Adult. *Chronic Obstructive Pulmonary Diseases: Journal of the COPD Foundation* 3: 668-682.

- (41) Crystal, R. G. Augmentation treatment for alpha1 antitrypsin deficiency. *Lancet* 2015; 386: 318-320.
- (42) De Bishnu, P., Hackett, N. R., Crystal, R. G. & Boyer, J. L. Rapid/sustained anti-anthrax passive immunity mediated by co-administration of Ad/AAV. *Molecular Therapy* 2008; 16: 203-209.
- (43) Chiuchiolo, M. J. *et al.* Intrapleural administration of an AAVrh. 10 vector coding for human  $\alpha$ 1-antitrypsin for the treatment of  $\alpha$ 1-antitrypsin deficiency. *Human Gene Therapy Clinical Development* 2013; 24: 161-173.
- (44) Mueller, C. *et al.* Human Treg responses allow sustained recombinant adeno-associated virus-mediated transgene expression. *The Journal of clinical investigation* 2013; 123: 5310-5318.
- (45) Yusa, K. *et al.* Targeted gene correction of [agr]1-antitrypsin deficiency in induced pluripotent stem cells. *Nature* 2011; 478: 391-394.
- (46) Rashid, S. T. & Lomas, D. A. Stem cell-based therapy for  $\alpha$ (1)-antitrypsin deficiency. *Stem Cell Research & Therapy* 2012; 3: 1.
- (47) Miller, M. R. *et al.* Standardisation of spirometry. *Eur Respir J* 2005; 26: 319-338.
- (48) Wedzicha, J. The heterogeneity of chronic obstructive pulmonary disease. *Thorax* 2000; 55: 631-632.
- (49) Agusti, A. *et al.* Characterisation of COPD heterogeneity in the ECLIPSE cohort. *Respiratory research* 2010; 11: 1.
- (50) Criée, C. *et al.* Body plethysmography—its principles and clinical use. *Respiratory medicine* 2011; 105: 959-971.
- (51) Macintyre, N. *et al.* Standardisation of the single-breath determination of carbon monoxide uptake in the lung. *European Respiratory Journal* 2005; 26: 720-735.
- (52) Kaminsky, D. A., Whitman, T. & Callas, P. W. DLCO versus DLCO/VA as predictors of pulmonary gas exchange. *Respiratory medicine* 2007; 101: 989-994.
- (53) Hughes, J. M. B. & Pride, N. B. Examination of the carbon monoxide diffusing capacity (DLCO) in relation to its KCO and VA components. *American journal of respiratory and critical care medicine* 2012; 186: 132-139.
- (54) Hathaway, E. H., Tashkin, D. & Simmons, M. S. Intraindividual Variability in Serial Measurements of OLeo and Alveolar Volume over One Year in Eight Healthy Subjects Using Three Independent Measuring Systems. *Am Rev Respir Dis* 1989; 140: 1818-1822.

- (55) Pellegrino, R. *et al.* Interpretative strategies for lung function tests. *European Respiratory Journal* 2005; 26: 948-968.
- (56) Borg, G. A. Psychophysical bases of perceived exertion. *Med sci sports exerc* 1982; 14: 377-381.
- (57) Laboratories, A. C. o. P. S. f. C. P. F. ATS statement: guidelines for the six-minute walk test. *American journal of respiratory and critical care medicine* 2002; 166: 111.
- (58) Enright, P. L. The six-minute walk test. *Respiratory care* 2003; 48: 783-785.
- (59) Jones, P. W., Quirk, F. H., Baveystock, C. M. & Littlejohns, P. A self-complete measure of health status for chronic airflow limitation: the St. George's Respiratory Questionnaire. *American Review of Respiratory Disease* 1992; 145: 1321-1327.
- (60) Rogalla, P., Kloeters, C. & Hein, P. A. CT technology overview: 64-slice and beyond. *Radiologic clinics of North America* 2009; 47: 1-11.
- (61) Hu, S., Hoffman, E. A. & Reinhardt, J. M. Automatic lung segmentation for accurate quantitation of volumetric X-ray CT images. *IEEE transactions on medical imaging* 2001; 20: 490-498.
- (62) Zach, J. A. *et al.* Quantitative CT of the Lungs and Airways in Healthy Non-Smoking Adults. *Investigative radiology* 2012; 47: 596.
- (63) Gevenois, P. A. *et al.* Comparison of computed density and microscopic morphometry in pulmonary emphysema. *Am J Respir Crit Care Med* 1996; 154: 187-192.
- (64) Bankier, A. A., De Maertelaer, V., Keyzer, C. & Gevenois, P. A. Pulmonary Emphysema: Subjective Visual Grading versus Objective Quantification with Macroscopic Morphometry and Thin-Section CT Densitometry 1. *Radiology* 1999; 211: 851-858.
- (65) Gevenois, P. A., De Maertelaer, V., De Vuyst, P., Zanen, J. & Yernault, J.-C. Comparison of computed density and macroscopic morphometry in pulmonary emphysema. *American journal of respiratory and critical care medicine* 1995; 152: 653-657.
- (66) Park, K. J., Bergin, C. J. & Clausen, J. L. Quantitation of Emphysema with Three-dimensional CT Densitometry: Comparison with Two-dimensional Analysis, Visual Emphysema Scores, and Pulmonary Function Test Results 1. *Radiology* 1999; 211: 541-547.
- (67) Galbán, C. J. *et al.* Computed tomography-based biomarker provides unique signature for diagnosis of COPD phenotypes and disease progression. *Nature medicine* 2012; 18: 1711-1715.

- (68) Mull, R. T. Mass estimates by computed tomography: physical density from CT numbers. *American journal of roentgenology* 1984; 143: 1101-1104.
- (69) Heremans, A., Verschakelen, J. A. & Demedts, M. Measurement of lung density by means of quantitative CT scanning: a study of correlations with pulmonary function tests. *Chest* 1992; 102: 805-811.
- (70) Mishima, M. *et al.* Complexity of terminal airspace geometry assessed by lung computed tomography in normal subjects and patients with chronic obstructive pulmonary disease. *Proceedings of the National Academy of Sciences* 1999; 96: 8829-8834.
- (71) Litzlbauer, H. D. *et al.* Synchrotron-Based Micro-CT Imaging of the Human Lung Acinus. *The Anatomical Record* 2010; 293: 1607-1614.
- (72) Parameswaran, H. *et al.* Three-dimensional measurement of alveolar airspace volumes in normal and emphysematous lungs using micro-CT. *Journal of Applied Physiology* 2009; 107: 583-592.
- (73) Litzlbauer, H. D. *et al.* Three-dimensional imaging and morphometric analysis of alveolar tissue from microfocal X-ray-computed tomography. *American Journal of Physiology-Lung Cellular and Molecular Physiology* 2006; 291: L535-L545.
- (74) Tanabe, N. *et al.* MicroCT Comparison of Preterminal Bronchioles in Centrilobular and Panlobular Emphysema. *American Journal of Respiratory And Critical Care Medicine* 2016.
- (75) Holdsworth, D. W. & Thornton, M. M. Micro-CT in small animal and specimen imaging. *Trends in Biotechnology* 2002; 20: S34-S39.
- (76) Ritman, E. L. Micro-computed tomography of the lungs and pulmonary-vascular system. *Proceedings of the American Thoracic Society* 2005; 2: 477-480.
- (77) Cutillo, A. G. & Armonk, M. *Application of magnetic resonance to the study of lung.* (Fortuna, 1996).
- (78) Albert, M. *et al.* Biological magnetic resonance imaging using laser-polarized  $^{129}\text{Xe}$ . 1994.
- (79) Möller, H. E. *et al.* MRI of the lungs using hyperpolarized noble gases. *Magnetic Resonance in Medicine* 2002; 47: 1029-1051.
- (80) Bauman, G. *et al.* Non-contrast-enhanced perfusion and ventilation assessment of the human lung by means of fourier decomposition in proton MRI. *Magnetic resonance in medicine* 2009; 62: 656-664.
- (81) Bergin, C., Pauly, J. & Macovski, A. Lung parenchyma: projection reconstruction MR imaging. *Radiology* 1991; 179: 777-781.

- (82) Heinrich, M. P. *et al.* MIND: Modality independent neighbourhood descriptor for multi-modal deformable registration. *Medical Image Analysis* 2012; 16: 1423-1435.
- (83) Capaldi, D. P. *et al.* Free-breathing Pulmonary 1 H and Hyperpolarized 3 He MRI: Comparison in COPD and Bronchiectasis. *Academic radiology* 2015; 22: 320-329.
- (84) Ma, W. *et al.* Ultra-short echo-time pulmonary MRI: Evaluation and reproducibility in COPD subjects with and without bronchiectasis. *Journal of Magnetic Resonance Imaging* 2015; 41: 1465-1474.
- (85) Sheikh, K. *et al.* Ultrashort echo time MRI biomarkers of asthma. *Journal of Magnetic Resonance Imaging* 2016.
- (86) Walker, T. G. & Happer, W. Spin-exchange optical pumping of noble-gas nuclei. *Reviews of Modern Physics* 1997; 69: 629.
- (87) Kirby, M. *et al.* Hyperpolarized 3He magnetic resonance functional imaging semiautomated segmentation. *Academic radiology* 2012; 19: 141-152.
- (88) Parraga, G., Mathew, L., Etemad-Rezai, R., McCormack, D. G. & Santyr, G. E. Hyperpolarized 3He magnetic resonance imaging of ventilation defects in healthy elderly volunteers: initial findings at 3.0 Tesla. *Academic radiology* 2008; 15: 776-785.
- (89) Svenningsen, S., Nair, P., Guo, F., McCormack, D. G. & Parraga, G. Is ventilation heterogeneity related to asthma control? *European Respiratory Journal* 2016; ERJ-00393-02016.
- (90) de Lange, E. E. *et al.* Evaluation of asthma with hyperpolarized helium-3 MRI: correlation with clinical severity and spirometry. *CHEST Journal* 2006; 130: 1055-1062.
- (91) Altes, T. A. *et al.* Hyperpolarized 3He MR lung ventilation imaging in asthmatics: preliminary findings. *Journal of Magnetic Resonance Imaging* 2001; 13: 378-384.
- (92) Costella, S. *et al.* Regional pulmonary response to a methacholine challenge using hyperpolarized 3He magnetic resonance imaging. *Respirology* 2012; 17: 1237-1246.
- (93) Stejskal, E. O. & Tanner, J. E. Spin diffusion measurements: spin echoes in the presence of a time-dependent field gradient. *The journal of chemical physics* 1965; 42: 288-292.
- (94) Saam, B. T. *et al.* MR imaging of diffusion of 3He gas in healthy and diseased lungs. *Magnetic Resonance in Medicine* 2000; 44: 174-179.
- (95) Jones, D. K. *Diffusion mri.* (Oxford University Press, 2010).

- (96) Woods, J. C. *et al.* Hyperpolarized <sup>3</sup>He diffusion MRI and histology in pulmonary emphysema. *Magn Reson Med* 2006; 56: 1293-1300.
- (97) Kirby, M. *et al.* Hyperpolarized <sup>3</sup>He and <sup>129</sup>Xe magnetic resonance imaging apparent diffusion coefficients: physiological relevance in older never-and ex-smokers. *Physiological reports* 2014; 2: e12068.
- (98) Waters, B., Owers-Bradley, J. & Silverman, M. Acinar structure in symptom-free adults by Helium-3 magnetic resonance. *American journal of respiratory and critical care medicine* 2006; 173: 847-851.
- (99) Fain, S. B. *et al.* Detection of age-dependent changes in healthy adult lungs with diffusion-weighted <sup>3</sup>He MRI. *Academic radiology* 2005; 12: 1385-1393.
- (100) Altes, T. A., Mata, J., de Lange, E. E., Brookeman, J. R. & Mugler, J. P., 3rd. Assessment of lung development using hyperpolarized helium-3 diffusion MR imaging. *J Magn Reson Imaging* 2006; 24: 1277-1283.
- (101) Kaushik, S. S. *et al.* Diffusion-weighted hyperpolarized <sup>129</sup>Xe MRI in healthy volunteers and subjects with chronic obstructive pulmonary disease. *Magnetic resonance in medicine* 2011; 65: 1154-1165.
- (102) Kirby, M. *et al.* Hyperpolarized <sup>3</sup>He and <sup>129</sup>Xe MR Imaging in Healthy Volunteers and Patients with Chronic Obstructive Pulmonary Disease. *Radiology* 2012; 265: 600-610.
- (103) Driehuys, B. *et al.* Chronic obstructive pulmonary disease: safety and tolerability of hyperpolarized <sup>129</sup>Xe MR imaging in healthy volunteers and patients. *Radiology* 2012; 262: 279-289.
- (104) Thomen, R. P. *et al.* Direct comparison of <sup>129</sup>Xe diffusion measurements with quantitative histology in human lungs. *Magnetic resonance in medicine* 2016.
- (105) Sukstanskii, A. L. & Yablonskiy, D. A. In vivo lung morphometry with hyperpolarized <sup>3</sup>He diffusion MRI: theoretical background. *J Magn Reson* 2008; 190: 200-210.
- (106) Yablonskiy, D. A. *et al.* Quantification of lung microstructure with hyperpolarized <sup>3</sup>He diffusion MRI. *J Appl Physiol* 2009; 107: 1258-1265.
- (107) Paulin, G. A. *et al.* Noninvasive quantification of alveolar morphometry in elderly never-and ex-smokers. *Physiological reports* 2015; 3: e12583.
- (108) Quirk, J. D. *et al.* Experimental evidence of age-related adaptive changes in human acinar airways. *Journal of Applied Physiology* 2016; 120: 159-165.



## 2 Chapter 2: Pulmonary $^3\text{He}$ Magnetic Resonance Imaging Biomarkers of Emphysema in Alpha-1 Antitrypsin Deficiency

*The contents of this chapter have been accepted to Academic Radiology as an original research article authored by Eric Lessard, Heather M Young, Anurag Bhalla, Damien Pike, Khadija Sheikh, David G McCormack, Alexei Ouriadov and Grace Parraga titled Pulmonary  $^3\text{He}$  Magnetic Resonance Imaging Biomarkers of Regional Airspace Enlargement in Alpha-1 Antitrypsin Deficiency. To better understand AATD related emphysema as measured by diffusion-weighted MRI we evaluated a small group of subjects with AATD using diffusion-weighted MRI, CT, spirometry, plethysmography and DLco. We compared these measurements to those obtained in ex-smokers with smoking related emphysema and healthy age-matched never-smokers.*

### 2.1 Introduction

Alpha-1 Antitrypsin Deficiency (AATD), first described by Laurell and Eriksson in 1963,<sup>1</sup> is an autosomal co-dominant hereditary disorder caused by a mutation in the SERPINA1 gene, which leads to dysregulation of neutrophil elastase.<sup>2</sup> This commonly manifests as early-onset panlobular emphysema and affects approximately 1/5000 North Americans.<sup>2,3</sup> Respiratory failure accounts for 45-72% of deaths in patients with AATD. Importantly, an increased risk of mortality may be predicted using CT biomarkers of emphysema<sup>2</sup> and overall, outcomes are worse when patients cannot access augmentation therapy.<sup>4</sup>

As is the case for smoking-related emphysema, there is no cure for AATD, although current AATD treatments aimed at slowing disease progression include exogenous alpha-1 antitrypsin augmentation therapy. X-ray computed tomography (CT) lung density measurements showed that augmentation therapy may slow the rate of emphysema progression in AATD patients<sup>4</sup> - an important finding that may help guide treatment decisions given the high cost of intravenous augmentation treatment.<sup>2</sup> However, while the CT measurement of emphysema progression was significantly lower in the treatment arm of the RAPID study, this did not correlate with similar changes in patient-related quality-of-life measurements.<sup>4</sup> This important limitation is also motivating the development of novel biomarkers and intermediate endpoints of AATD emphysema for novel treatments including gene therapy<sup>5</sup> and pluripotent stem cells.<sup>6,7</sup>



The decline over time of the forced expiratory volume in 1 second ( $FEV_1$ )<sup>8-10</sup> and the diffusing capacity of carbon monoxide ( $DL_{CO}$ ) are both considered as biomarkers of AATD lung disease. While highly variable,<sup>11</sup>  $DL_{CO}$  measurements correlate with pathology measurements<sup>12</sup> and CT emphysema findings<sup>13</sup> such as the relative area of the CT density histogram  $\leq -950$  Hounsfield units ( $RA_{950}$ ).<sup>14</sup> More recently, pulmonary imaging biomarkers that exploit the diffusive motion of inhaled polarized gases such as  $^3He$ <sup>15</sup> and  $^{129}Xe$ <sup>16</sup> have been measured in patients with emphysema<sup>17</sup> using diffusion-weighted MRI pulse sequences.

In particular, the  $^3He$  MRI apparent diffusion coefficient (ADC) was shown to reflect emphysema.<sup>15,18</sup> Multiple b-value diffusion-weighted lung MRI<sup>17</sup> also provides estimates of airway space geometry,<sup>17,19</sup> based on the heterogeneous gas displacement in the terminal airways that are assumed to be cylindrical in shape.<sup>20</sup> Such non-invasive MRI morphometry estimates<sup>17</sup> provide a way to bypass or obviate the necessity for pathological analyses<sup>21-24</sup> and may offer crucial information about lung disease progression, as well as treatment response. Previous MRI studies in AATD patients<sup>25-28</sup> showed there was no statistical difference in ADC values after two-years of follow-up<sup>26</sup> but unfortunately, no morphometry data were acquired. MRI morphometry modelling approaches were recently evaluated in COPD and AATD patients,<sup>29</sup> but this work did not evaluate clinical and other regional biomarkers. This is important because for AATD patients, emphysematous tissue destruction ensues early in life and panlobular emphysema is often severe by middle-age.

Therefore, the aim of this study was to evaluate AATD patients using multiple b-value diffusion-weighted MRI as well as pulmonary function and CT measurements of emphysema. We hypothesized that MRI measurements would be highly sensitive to airspace enlargement which would be significantly worse in AATD patients as compared to clinically similar ex-smokers with COPD.

## 2.2 Materials and Methods

### 2.2.1 Study Volunteers and Design

All participants provided written informed consent to a study protocol approved by a local research ethics board and Health Canada. Patients aged 40-90 years of age with a diagnosis of AATD and ex-smokers with COPD, >10 pack-years smoking history and CT evidence of emphysema were recruited from a tertiary care centre and evaluated using spirometry, plethysmography, thoracic imaging, the St. George's Respiratory Questionnaire (SGRQ) and 6-minute walk test (6MWT) during a single two-hour visit. CT evidence of emphysema was defined as an  $RA_{950} \geq 6.8\%$  as previously described.<sup>30</sup> Older never-smokers were also enrolled aged 60-80 years, <0.5 pack-years and no history of chronic lung disease or uncontrolled cardiovascular disease and completed all study measurements except for the SGRQ and 6MWT.

### 2.2.2 Spirometry, Plethysmography, SGRQ and 6MWT

Spirometry measurements were acquired according to the American Thoracic Society (ATS) guidelines<sup>31</sup> using a whole body system (MedGraphics Corporation, St Paul, Minnesota, USA). Body plethysmography was also performed for the measurement of lung volumes and DLCO was measured using the attached gas analyzer. The SGRQ<sup>32</sup> was used to establish overall quality of life and the 6MWT<sup>33</sup> was used to measure exercise capacity.

### 2.2.3 Image Acquisition

MRI was performed on a whole body 3T system (MR750 Discovery, GEHC, Milwaukee, WI) with broadband imaging capability.<sup>34</sup> <sup>3</sup>He MRI employed a whole body gradient set with maximum gradient amplitude of 50mT/m and a single-channel, rigid elliptical transmit/receive chest coil (RAPID Biomedical GmbH, Wuerzburg, Germany). The basis frequency of the coil was 97.3 MHz and excitation power was 3 kW using an AMT 3T90 RF power amplifier (GEHC). Subjects were positioned supine in the scanner for both <sup>1</sup>H and <sup>3</sup>He MRI and instructed by a pulmonary function technologist to inhale a 1L gas mixture of <sup>3</sup>He/N<sub>2</sub> (20% <sup>3</sup>He by volume) from functional residual capacity (FRC), ensuring

a self-consistent lung volume of FRC+1L, with image acquisition performed under breath-hold conditions as previously described.<sup>34</sup> <sup>3</sup>He gas was polarized to 30-40% polarization using a spin-exchange optical polarizer (Polarean Inc, Durham, NC). Diffusion-weighted <sup>3</sup>He MRI data were acquired using a multi-slice interleaved 2D gradient echo diffusion-weighted sequence with a matrix size of 128x80, for seven 30mm coronal slices (900 $\mu$ s selective RF pulse, flip angle  $\theta = 4^\circ$ , TE = 3.9ms, TR=5.6ms, bandwidth=62.5kHz, in-plane resolution = 3.125x3.125 mm<sup>2</sup>, b=0, 1.6, 3.2, 4.8, 6.4 s/cm<sup>2</sup>); the diffusion-sensitization gradient pulse ramp up/down time was 500 $\mu$ s with a diffusion time of 1460 $\mu$ s. The potential for image artifacts associated with RF pulse “history”<sup>35</sup> was addressed by using an optimal constant flip angle (4 degrees).<sup>36</sup> A diffusion-sensitizing, gradient-step, k-space acquisition scheme starting at the maximum b-value was used to ensure that maximum MR signal was acquired for diffusion-weighted images at greater b-values. All five b-value images were acquired during a single 15s breath-hold.

Thoracic CT was acquired on a 64-slice Lightspeed VCT scanner (General Electric Health Care, Milwaukee, Wisconsin) (64  $\times$  0.625 mm, 120 kVp, 100 effective mA, tube rotation time=500 msec, and a pitch=1.0). A single spiral acquisition was performed with subjects in the supine position and at inspiration breath-hold after inhalation of a 1.0L N<sub>2</sub> bag from FRC (NS, AATD1, 6-8) or at full inspiration (COPD, AATD2-5). CT Images were reconstructed using a slice thickness of 1.25 mm with a standard convolution kernel. The total effective dose for an average participant was 1.8 mSv according to manufacturer settings and Imaging Performance Assessment of CT (ImPACT) CT patient dosimetry calculator based on software from the Health Protection Agency of the United Kingdom (NRPB-SR250).

#### 2.2.4 Image Analysis

To measure MRI ventilation defect percent (VDP), we used semi-automated segmentation software (MATLAB R2014b; MathWorks, Natick, Mass) as previously described,<sup>37</sup> utilizing an independently acquired image without diffusion weighting. <sup>3</sup>He MRI ADC maps were generated as described previously<sup>38,39</sup> and the Weibel acinar duct model<sup>20</sup> was used to generate morphometry estimates as previously described.<sup>17,23,40</sup> Multiple-b-value

measurements<sup>39</sup> of the <sup>3</sup>He diffusion-attenuated MR signal were used to derive morphological parameters of the acinar airway, including external radius (R), internal radius (r), alveolar length (L), depth of alveolar sleeve (h), surface area-to-volume ratio (S/V) and mean linear intercept (L<sub>m</sub>). To model the severe emphysema that accompanies AATD lung disease, we did not constrain R or r, nor their ratio, unlike previous work in elderly never-smokers and COPD patients.<sup>39</sup> The cylindrical model was used based on previous work<sup>17,41,42</sup> and based on the fact that in AATD patients, normal lung development and alveolarization is expected.<sup>43</sup> Regional ADC and morphometry measurements were computed using custom-built software generated using MATLAB software whereby the carina was identified in the b = 0 image and used to segment the lung into apical and basal regions.

CT airway count, RA<sub>950</sub>, and low attenuating clusters (LAC) with CT density values  $\leq -950$  HU<sup>44</sup> were determined using Pulmonary Workstation 2.0 (VIDA Diagnostics Inc., Coralville, IA). LAC was calculated using the log-log relationship<sup>44</sup> between the cumulative frequency distribution of emphysematous lesions (# of lesions) and cluster size (size of lesions) according to the power law relationship  $Y = X^{LAC}$  (Y = cumulative frequency distribution, X = size of lesions). Lower LAC values (more negative) are indicative of smaller, and fewer, clusters of emphysematous lesions whereas greater LAC values suggest fewer and larger lesions. Graphically, this is illustrated as spheres representing the relative size of emphysematous lesions, with larger spheres indicating larger and connected low attenuating areas. Regional RA<sub>950</sub> was generated using the carina to segment the lung into apical and basal lung regions.

### 2.2.5 Statistical Analysis

All statistical analyses were performed using IBM SPSS Statistics, Version 24 (IBM, Armonk, NY, USA). Comparisons between groups were performed using a multivariate analysis of variance (MANOVA) with post-hoc Tukey honest significant difference test. Results were considered significant when the probability of making a Type 1 error was < 5% (p < .05).

## 2.3 Results

Table 1 provides demographic information for the AATD patient subgroup (n=8, 57±7 years), ex-smokers with COPD (n=8, 77±6 years) and never-smokers (n=5, 64±2 years). There was significantly different FEV<sub>1</sub> (p = .007), FEV<sub>1</sub>/FVC (p < .0001), RV (p = .03) and DL<sub>CO</sub> (p < .0001) for AATD patients as compared to never-smokers but there were no significant differences between AATD and COPD patients except for age (p < .0001) and SGRQ (p=.01). COPD patients were significantly older and had a significantly better SGRQ score indicating better quality of life.

**Table 2-1: Demographic and pulmonary function measurements**

Parameters (±SD)	Never-Smoker n=5	COPD Ex-Smoker n=8	AATD n=8	NS-COPD	NS-AATD	AATD-COPD
Female n	5	1	3	-	-	-
Age yr	64 (2)	77 (6)	57 (7)	<b>.001</b>	.2	<b>&lt;.0001</b>
BMI kg/m <sup>2</sup>	24 (2)	26 (3)	27 (5)	.8	.6	.9
FEV <sub>1</sub> % <sub>pred</sub>	101 (9)	72 (34)	47 (20)	.1	<b>.007</b>	.2
FVC % <sub>pred</sub>	96 (9)	94 (26)	78 (21)	.9	.4	.4
FEV <sub>1</sub> /FVC %	80 (1)	52 (11)	47 (12)	<b>&lt;.0001</b>	<b>&lt;.0001</b>	.8
RV % <sub>pred</sub>	84 (24)	147 (50)	170 (65)*	.1	<b>.03</b>	.7
TLC % <sub>pred</sub>	97 (13)	110 (15)	129 (37)*	.2	.2	.9
RV/TLC %	35 (6)	50 (11)	51 (13)*	.05	.06	.9
DL <sub>CO</sub> % <sub>pred</sub>	95 (14)	55 (16)	44 (19)*	<b>.002</b>	<b>&lt;.0001</b>	.4
6MWD m	ND	380 (88)	385 (80)	ND	ND	.9 <sup>††</sup>
SGRQ	ND	30 (18)	55 (17)	ND	ND	<b>.01<sup>††</sup></b>

FEV<sub>1</sub>=forced expiratory volume in 1 second; %<sub>pred</sub>=percent predicted; FVC=forced vital capacity; RV=residual volume; TLC=total lung capacity; DL<sub>CO</sub>=diffusing capacity of the lungs for carbon monoxide; 6MWD=six-minute walk distance; SGRQ=St. George's Respiratory Questionnaire total score. MANOVA between groups with post-hoc Tukey HSD for multiple comparisons. <sup>††</sup>Unpaired t-test between COPD and AATD; \*n=7.

Figure 1 shows CT airway trees and coronal centre slice low attenuating cluster maps as well as coronal centre slice MRI ventilation and ADC maps for representative participants in each subgroup. For the two representative never-smokers, there was little or no evidence of CT low attenuating regions or clusters while MRI ADC maps were homogeneous with normal ADC values and ventilation maps reflected relatively few, small

ventilation defects. In the two representative COPD patients, there were numerous CT low attenuating regions and low attenuating clusters with large ventilation defects and abnormal ADC values, mainly in the apical lung. In the two representative AATD patients, CT low attenuating regions and clusters dominated in the lower lobes and this was concomitant with highly abnormal MRI ADC values (shown in yellow), mainly in the basal lung.

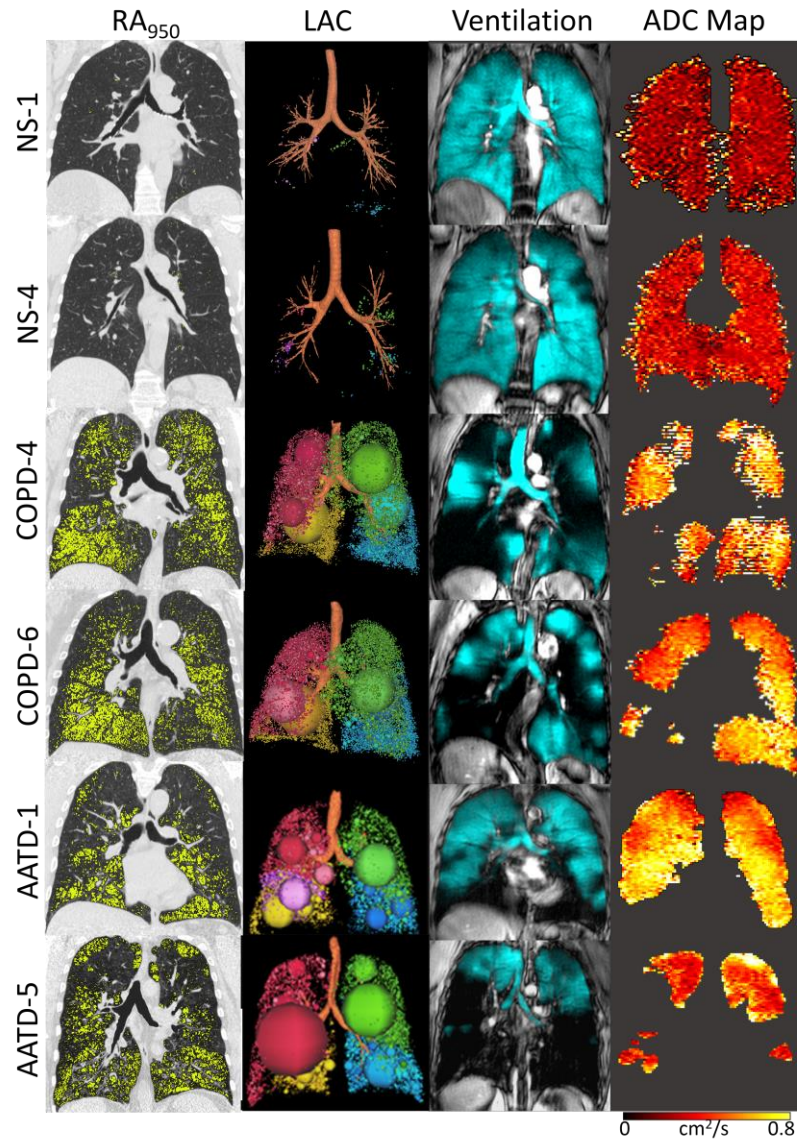


**Figure 2-1: Thoracic CT and MRI for Never-smokers, COPD and AATD Participants**

Left panels: CT RA<sub>950</sub> maps (yellow pixels corresponding to voxels <-950 Hounsfield Units) and CT LAC maps; Right panels: <sup>3</sup>He static ventilation (Cyan) co-registered with <sup>1</sup>H MRI; <sup>3</sup>He MRI apparent diffusion coefficient (ADC) maps. NS-1 is female age 63 years

with  $FEV_1=109\%$ pred,  $DLCO=103\%$ pred,  $RA_{950}=0.19\%$ ,  $ADC=0.25\text{ cm}^2/\text{s}$ ; NS-4 is female age 64 years with  $FEV_1=108\%$ pred,  $DLCO=99\%$ pred,  $RA_{950}=0.13\%$ ,  $ADC=0.29\text{ cm}^2/\text{s}$ ; COPD-4 is male age 75 years with  $FEV_1=30\%$ pred,  $DLCO=31\%$ pred,  $RA_{950}=26\%$ ,  $ADC=0.50\text{ cm}^2/\text{s}$ ; COPD-6 is male age 84 years with  $FEV_1=52\%$ pred,  $DLCO=47\%$ pred,  $RA_{950}=24\%$ ,  $ADC=0.50\text{ cm}^2/\text{s}$ ; AATD-1 is male age 67 with  $FEV_1=58\%$ pred,  $DLCO=50\%$ pred,  $RA_{950}=19\%$ ,  $ADC=0.57\text{ cm}^2/\text{s}$ ; AATD-5 is male age 50 with  $FEV_1=25\%$ pred,  $DLCO=32\%$ pred,  $RA_{950}=27\%$ ,  $ADC=0.47\text{ cm}^2/\text{s}$ .

Figure 2 shows the qualitative differences in  $RA_{950}$ , ADC and  $L_m$  maps for representative never-smokers, AATD and COPD patients. For example, for NS-2 and NS-5, there was no evidence, based on  $RA_{950}$  or MRI ADC, of airspace enlargement or emphysema. However, there was a difference in mean  $L_m$  for these two never-smokers with lower, darker voxels for NS-5, a female aged 63 years as compared to NS-2 a female never-smoker also aged 63 years and the reasons for these differences were not evident. For COPD and AATD patients, there was CT evidence of emphysema in the upper (COPD) and basal lung (AATD). ADC and  $L_m$  maps also show brighter colours that reflect enlarged airspaces that in COPD patients predominated in the upper lobes. In AATD-3, there was highly abnormal  $L_m$ , homogeneously distributed throughout the ventilated portions of the lung. For patient AATD-2, there was very poor basal lung ventilation and therefore no ADC or morphometry values could be reported from these regions, although CT showed moderate basal lung emphysema.

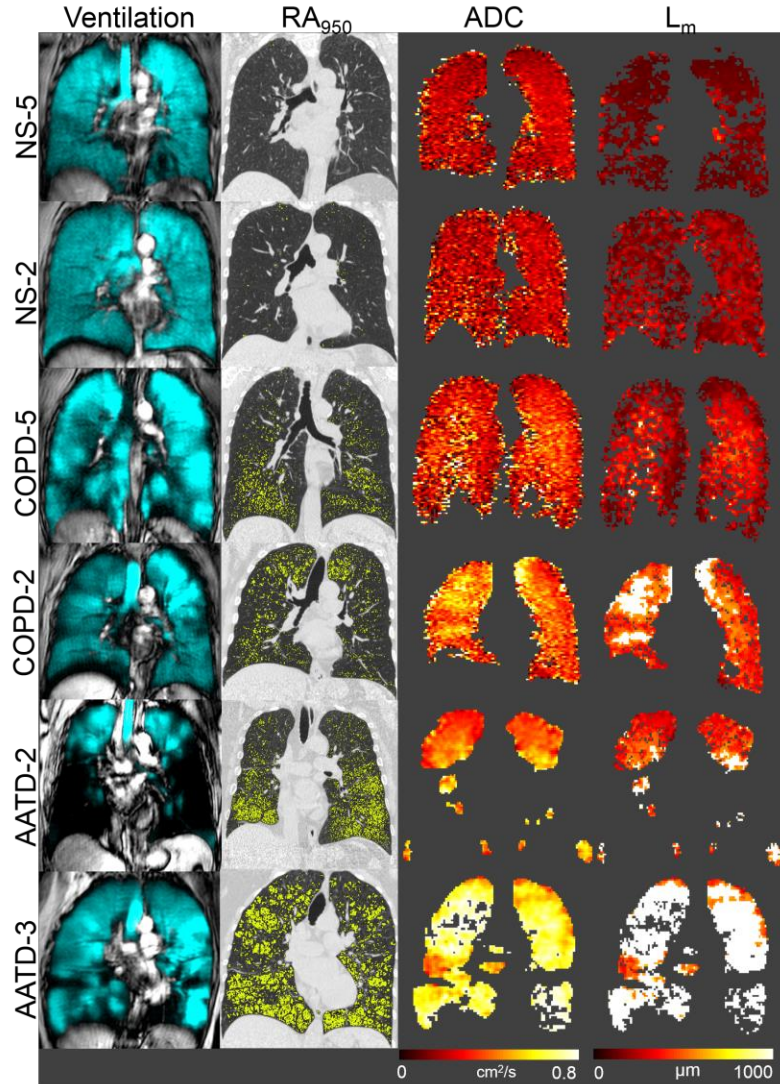


**Figure 2-2: Morphometry Maps for Representative Never-smokers, COPD ex-smokers and AATD Patients**

Left panels: MRI static ventilation (Cyan) co-registered with  $^1\text{H}$  MRI; CT  $\text{RA}_{950}$  maps (yellow pixels corresponding to voxels  $< 950$  Hounsfield Units). Right panels:  $^3\text{He}$  MRI apparent diffusion coefficient (ADC) and mean linear intercept ( $L_m$ ) maps. NS-5 is female age 63 years with  $\text{FEV}_1=106\%$ <sub>pred</sub>,  $\text{DLCO}=80\%$ <sub>pred</sub>,  $\text{RA}_{950}=0.19\%$ ,  $\text{ADC}=0.27\text{ cm}^2/\text{s}$ ,  $L_m=180\text{ }\mu\text{m}$ ; NS-2 is female age 63 years with  $\text{FEV}_1=94\%$ <sub>pred</sub>,  $\text{DLCO}=113\%$ <sub>pred</sub>,  $\text{RA}_{950}=0.44\%$ ,  $\text{ADC}=0.28\text{ cm}^2/\text{s}$ ,  $L_m=240\text{ }\mu\text{m}$ ; COPD-5 is female age 72 years with  $\text{FEV}_1=56\%$ <sub>pred</sub>,  $\text{DLCO}=59\%$ <sub>pred</sub>,  $\text{RA}_{950}=8\%$ ,  $\text{ADC}=0.33\text{ cm}^2/\text{s}$ ,  $L_m=310\text{ }\mu\text{m}$ ; COPD-2 is male age 79 years with  $\text{FEV}_1=126\%$ <sub>pred</sub>,  $\text{DLCO}=62\%$ <sub>pred</sub>,  $\text{RA}_{950}=11\%$ ,  $\text{ADC}=0.41\text{ cm}^2/\text{s}$ ,  $L_m=540\text{ }\mu\text{m}$ ; AATD-2 is male age 57 with  $\text{FEV}_1=37\%$ <sub>pred</sub>,  $\text{DLCO}=\text{ND}$ ,  $\text{RA}_{950}=23\%$ ,  $\text{ADC}=0.46\text{ cm}^2/\text{s}$ ,  $L_m=680\text{ }\mu\text{m}$ ; AATD-3 is female age 62 with  $\text{FEV}_1=61\%$ <sub>pred</sub>,  $\text{DLCO}=21\%$ <sub>pred</sub>,  $\text{RA}_{950}=31\%$ ,  $\text{ADC}=0.67\text{ cm}^2/\text{s}$ ,  $L_m=1200\text{ }\mu\text{m}$ .

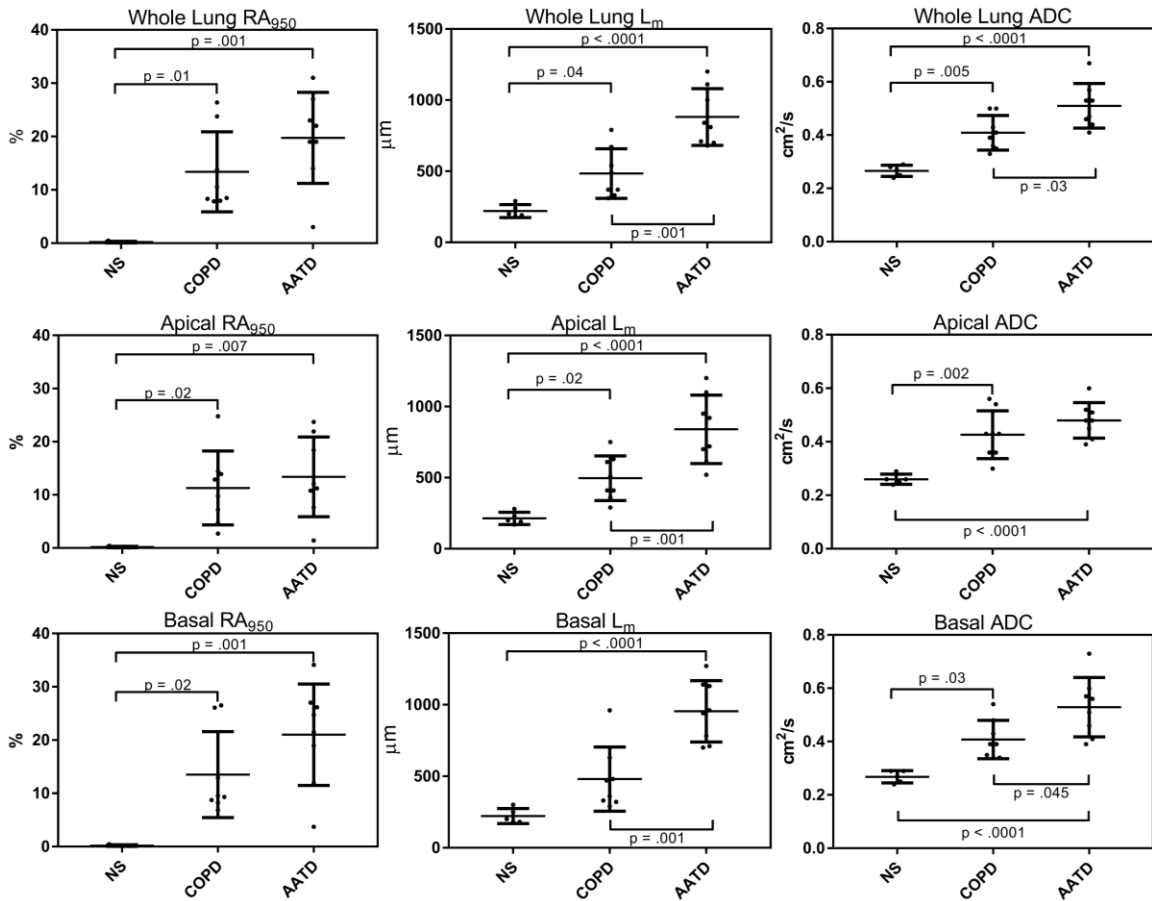


Table 2 and Figure 3 provide a summary of quantitative imaging measurements for each subgroup and Table 3 provides all imaging data by participant. As shown in Table 2, AATD subjects had significantly elevated whole lung ADC ( $p=.03$ ), basal lung ADC ( $p=.045$ )  $L_m$  ( $p=.001$ ) and diminished S/V ( $p=.01$ ) as compared to COPD ex-smokers.  $RA_{950}$  was significantly elevated in the basal portion of the lungs as compared to the apical portion in AATD subjects only ( $p = .03$ ). Figure 3 provides box and whisker plots for whole lung (top panel), apical (middle panel) and basal (bottom panel)  $RA_{950}$ ,  $L_m$  and ADC by subgroup. In COPD and AATD patients, there was significantly different whole lung, apical and basal  $L_m$  and ADC, but there was no significant difference in whole lung, apical or basal  $RA_{950}$ . Receiver operating curve (ROC) analysis was also performed between the AATD and COPD subgroups for  $L_m$ , (AUC = .95,  $p = .002$ ), ADC (AUC = .85,  $p = .02$ ) and  $RA_{950}$  (AUC = .71,  $p = .16$ ).

**Table 2-2: Pulmonary MRI and CT measurements**

Parameters ( $\pm$ SD)	Never-Smoker n=5	COPD Ex-Smoker n=8	AATD n=8	Significance of Difference (p)		
				NS-COPD	NS-AATD	AATD-COPD
WL ADC $cm^2/s$	.27 (.02)	.41 (.07)	.51 (.08)	<b>.005</b>	<b>&lt;.0001</b>	<b>.03</b>
Apical ADC $cm^2/s$	.26 (.02)	.42 (.07)	.48 (.07)	<b>.002</b>	<b>&lt;.0001</b>	.3
Basal ADC $cm^2/s$	.27 (.02)	.41 (.07)	.53 (.11)	<b>.03</b>	<b>&lt;.001</b>	<b>.045</b>
VDP %	2 (1)	23 (13)	28 (16)	<b>.03</b>	<b>.01</b>	.8
WL $L_m$ $\mu m$	220 (80)	480 (250)	890 (330)	<b>.04</b>	<b>&lt;.0001</b>	<b>.001</b>
Apical $L_m$ $\mu m$	210 (80)	500 (250)	840 (310)	<b>.02</b>	<b>&lt;.0001</b>	<b>.001</b>
Basal $L_m$ $\mu m$	220 (80)	480 (230)	950 (310)	.09	<b>&lt;.0001</b>	<b>.001</b>
S/V $cm^{-1}$	200 (50)	110 (50)	50 (20)	<b>&lt;.0001</b>	<b>&lt;.0001</b>	<b>.01</b>
WL CT $RA_{950}$ %	0.2 (0.2)	13 (8)	20 (9)	<b>.01</b>	<b>.001</b>	.3
Apical CT $RA_{950}$ %	0.2 (0.1)	11 (7)	13 (8)	<b>.02</b>	<b>.007</b>	.8
Basal CT $RA_{950}$ %	.2 (.2)	14 (8)	21 (10)	<b>.02</b>	<b>.001</b>	.2
CT LAC	-2.1 (.4)	-1.7 (.1)	-1.6 (.2)	.1	<b>.01</b>	.4
Airway count	151 (26)	112 (25)	120 (17)	<b>.02</b>	.1	.5

WL=whole lung; VDP=ventilation defect percent; ADC=apparent diffusion coefficient; R=external airway radius; r=internal airway radius; h=alveolar sheath;  $L_m$ =mean linear intercept;  $RA_{950}$ =relative area of the CT density histogram of attenuation values <-950 Hounsfield Units; LAC=low attenuating clusters. MANOVA between groups with post-hoc Tukey HSD for multiple comparisons.



**Figure 2-3: Regional Imaging Biomarkers**

Box and Whisker Plots show mean and standard deviation. NS=never-smoker, COPD=COPD ex-smoker, AATD=alpha-1 antitrypsin deficiency. RA<sub>950</sub>=relative area of the CT lung density histogram with attenuation values <-950 HU, L<sub>m</sub>=mean linear intercept, ADC=apparent diffusion coefficient. Group comparisons performed with an MANOVA and multiple comparisons corrected with a post-hoc Tukey HSD test.

**Table 2-3: MRI and CT Measurements by Participant**

Parameter (±SD)	ADC <sub>WL</sub> cm <sup>2</sup> /s	ADC <sub>Ap</sub> cm <sup>2</sup> /s	ADC <sub>Ba</sub> cm <sup>2</sup> /s	VDP %	L <sub>m(WL)</sub> μm	L <sub>m(Ap)</sub> μm	L <sub>m(Ba)</sub> μm	RA <sub>950</sub> %	LAC
NS-1	.25 (.04)	.25 (.03)	.25 (.04)	2	190 (80)	200 (90)	180 (70)	0.2	-1.6
NS-2	.28 (.04)	.26 (.03)	.29 (.04)	2	240 (80)	230 (70)	250 (90)	0.4	-2.4
NS-3	.24 (.02)	.24 (.02)	.24 (.02)	2	200 (60)	190 (50)	200 (60)	0.1	-2.4
NS-4	.29 (.03)	.29 (.03)	.29 (.03)	2	290 (80)	280 (80)	300 (80)	0.1	-1.6
NS-5	.27 (.03)	.26 (.02)	.27 (.03)	3	180 (90)	170 (70)	180 (100)	0.2	-2.3
<b>All NS</b>	<b>.27 (.02)</b>	<b>.26 (.02)</b>	<b>.27 (.02)</b>	<b>2 (1)</b>	<b>220 (80)</b>	<b>210 (80)</b>	<b>220 (80)</b>	<b>0.2 (0.2)</b>	<b>-2.1 (0.4)</b>
COPD-1	.36 (.05)	.36 (.05)	.35 (.05)	16	330 (130)	360 (150)	290 (110)	8	-1.9
COPD-2	.41 (.05)	.43 (.04)	.39 (.05)	16	540 (280)	610 (320)	470 (200)	11	-1.7
COPD-3	.35 (.03)	.36 (.03)	.34 (.04)	5	370 (150)	410 (160)	330 (120)	8	-1.9
COPD-4	.50 (.08)	.54 (.07)	.48 (.08)	45	670 (350)	750 (350)	630 (340)	26	-1.7
COPD-5	.33 (.04)	.30 (.04)	.34 (.04)	14	310 (120)	290 (110)	320 (130)	8	-1.9
COPD-6	.50 (.05)	.56 (.05)	.54 (.06)	31	790 (380)	630 (330)	960 (350)	24	-1.8
COPD-7	.39 (.07)	.43 (.08)	.39 (.07)	30	370 (220)	410 (220)	360 (210)	14	-1.6
COPD-8	.43 (.06)	.43 (.06)	.43 (.06)	25	490 (240)	510 (250)	480 (230)	8	-1.6
<b>All COPD</b>	<b>.41 (.07)</b>	<b>.42 (.07)</b>	<b>.41 (.07)</b>	<b>23 (13)</b>	<b>480 (250)</b>	<b>500 (250)</b>	<b>480 (230)</b>	<b>13 (8)</b>	<b>-1.7 (0.1)</b>
AATD-1	.57 (.09)	.51 (.06)	.60 (.13)	27	1000 (410)	920 (440)	1100 (330)	19	-1.4
AATD-2	.46 (.08)	.39 (.07)	.51 (.10)	53	680 (320)	610 (280)	940 (350)	23	-1.9
AATD-3	.67 (.10)	.60 (.08)	.73 (.12)	13	1200 (360)	1200 (380)	1270 (330)	31	-1.3
AATD-4	.53 (.08)	.52 (.07)	.56 (.08)	17	1110 (220)	1070 (220)	1140 (210)	19	-1.5
AATD-5	.47 (.12)	.48 (.10)	.46 (.12)	49	700 (350)	700 (360)	700 (340)	27	-1.6
AATD-6	.41 (.09)	.41 (.06)	.41 (.10)	10	710 (190)	720 (190)	710 (190)	3	-1.9
AATD-7	.44 (.09)	.48 (.06)	.39 (.12)	21	840 (260)	950 (240)	780 (240)	14	-1.4
AATD-8	.53 (.04)	.45 (.03)	.57 (.05)	37	810 (440)	520 (270)	960 (430)	22	-1.7
<b>All AATD</b>	<b>.51 (.08)</b>	<b>.48 (.07)</b>	<b>.53 (.11)</b>	<b>28 (16)</b>	<b>890 (330)</b>	<b>840 (310)</b>	<b>950 (310)</b>	<b>20 (9)</b>	<b>-1.6 (0.2)</b>

SD=standard deviation; ADC=apparent diffusion coefficient; WL=whole lung; Ap=apical lung; Ba=basal lung; VDP=ventilation defect percent; L<sub>m</sub>=mean linear intercept; S/V=surface to volume ratio; RA<sub>950</sub>=relative area of the CT density histogram with attenuation values < -950 HU; LAC=low attenuating clusters

## 2.4 Discussion

For patients with AATD, pulmonary function tests and thoracic CT measurements of emphysema are typically used to evaluate disease severity, disease progression and response to therapy. Unfortunately, such measurements are relatively insensitive to small changes over time and do not fully explain longitudinal changes in symptoms and quality of life. Therefore, here our objective was to evaluate inhaled-gas MRI biomarkers of emphysema in AATD patients and compare these with CT and other clinical measurements of emphysema in elderly never-smokers and COPD patients with smoking-related emphysema.<sup>21,23</sup> We measured MRI and CT biomarkers of emphysema and observed: 1) abnormal MRI ADC and  $L_m$  measurements that were significantly worse in AATD as compared to COPD patients in whom CT  $RA_{950}$ , airway count and other pulmonary function test measurements were not significantly different, 2) differences in ADC and  $L_m$  in elderly never-smokers with normal CT, reflecting different senile emphysematous changes, and, 3) highly abnormal basal lung MRI  $L_m$  values in AATD patients although there was no basal lung ventilation in some AATD patients.

As might be expected, in AATD patients, MRI measurements of ventilation (VDP) and parenchyma microstructure (ADC) were abnormally elevated in the basal lung. Ventilation defects were prominent in participants AATD-1, AATD-2 and AATD-5 and this was consistent with the notion that in severe emphysema, the time constants for lung filling were longer than the MRI acquisition timeframe. Ventilation defects were also spatially related to regions with abnormal  $RA_{950}$  and this was previously shown in severe COPD.<sup>45,46</sup> In particular, in patient AATD-2, there were large ventilation defects, which was coincident with a highly abnormal SGRQ score of 80. It is important to note that in this patient,  $FEV_1$  did not reflect the severity of emphysema, nor symptoms. In contrast, for Subject AATD-6, there was imaging evidence of very mild emphysema and this was in agreement with modestly abnormal SGRQ, 6MWD and  $DL_{CO}$  values.

We were surprised to observe that there was no difference in pulmonary function test and CT biomarkers of emphysema in AATD patients compared to COPD ex-smokers in whom there were significantly different  $L_m$ , S/V and ADC (WL and basal) measurements. This

may be due to different underlying pathophysiological mechanisms for panlobular emphysema, common in AATD patients, as compared to centrilobular emphysema more common in current or previous smokers without AATD. There was no difference in airway count between the COPD and AATD subgroups. This is somewhat surprising because airway count has been suggested as a unique biomarker of COPD in smokers and ex-smokers and is an independent predictor of BMI, airflow obstruction, dyspnea, and exercise capacity (BODE) index<sup>47</sup> in COPD patients. The airway count result may stem from a small sample size but we also note that there was a difference between COPD and NS participants for airway count. This may suggest that similar to ex-smokers with COPD, in AATD emphysema, terminal airways are also occluded or obliterated so that they cannot be resolved using CT. To our knowledge this is a novel result. It is also noteworthy that for AATD patients with greater overall MRI evidence of airspace enlargement, suggestive of emphysema, there was greater apical lung ADC which supports the notion that as AATD worsens, both the basal and apical lung are involved. It is important to point out however that not all AATD patients present with basal-dominant emphysema<sup>48</sup> and this was also observed here in AATD-7, with greater apical as compared to basal ADC and  $L_m$ . Elevated apical  $L_m$  and ADC in AATD-7 may be explained by a 43 pack-year smoking history, although there is no apical-dominant disease in patient AATD-3 (35 pack years) or patient AATD-8 (30 pack years). Furthermore, the range of  $L_m$  and ADC values for NS may be indicative of different senile emphysematous changes. While NS-1 and NS-5 both have smaller airspaces as measured by MRI than age matched NS-4 who has airspaces approximately 50% larger (190 $\mu$ m vs 290 $\mu$ m). The reasons for this difference is not clear, but differences in unappreciated environmental exposures or other undetermined causes of accelerated lung aging in these individuals is possible.

While these cross-sectional results provide good evidence of the feasibility of acquiring MRI biomarkers in AATD patients, they also provide a better understanding of regional emphysema and the relationship of emphysema with quality of life in these patients. For example, perhaps because of the small sample size, SGRQ was the only clinical measurement that was significantly different in COPD and AATD patients. This finding is consistent with previous work that showed the relationship of modestly diminished  $DL_{CO}$

with MRI biomarkers in ex-smokers with normal spirometry but abnormal SGRQ and 6MWD.<sup>49</sup> The elevated  $L_m$ , ADC and S/V measurements in AATD patients here also revealed the sensitivity of MRI biomarkers to subtle differences in airspace enlargement even in the absence of CT measurement differences. Our results suggest that ADC may better distinguish airspace enlargement observed in NS participants and COPD participants while  $L_m$  may better distinguish between emphysematous lesions in COPD and AATD patients. We note that previous work<sup>50</sup> reported a similar finding for ADC and  $L_m$  in ex-smokers with and without emphysema using ROC analysis with AUC = .9 (p=.002) for ADC, and .91 (p=.02) for  $L_m$ , respectively. Taken together, these data suggest that MRI-derived  $L_m$  captures subtle differences between panlobular (AATD) and centrilobular (COPD) emphysema. We think the sensitivity of MRI can play an important role in measuring disease progression in longitudinal studies or response to therapy in clinical trials with small sample sizes, such as evaluated here. Similar to CT biomarkers of emphysema, MRI biomarkers of airspace enlargement may play an important role in measuring emphysema in AATD patients undergoing augmentation therapy which is especially important given the high cost of treatment.

We must acknowledge a number of study limitations and caveats. It is important to note that a shortcoming of inhaled gas MRI is the reliance of measurements on lung regions that are well-ventilated. In other words, where there are ventilation defects, no values can be reported; this generates a bias towards normal values from ventilated lung (in this case, apical lung). Furthermore, for longitudinal evaluation it is important to ensure that lung inflation levels is consistent between scans, such as in the RAPID trial<sup>4</sup>, and this would certainly help with reproducibility and measurement precision. It is also important to note that diffusion-weighted MRI reproducibility was previously evaluated by three different groups including the measurement of precision of ADC values (28, 51, 52) and  $L_m$  values (53). These previous results provided a strong foundation for our approach and for future longitudinal studies. These factors are important to consider if the techniques evaluated here are to be used clinically to monitor disease progression in AATD patients over time and those undergoing augmentation therapy. Using CT emphysema measurements, augmentation therapy has been shown to slow the rate of lung tissue density loss and we

expect that MRI biomarker sensitivity can also be exploited for longitudinal evaluations of this patient population. We also note that for one participant who was severely impaired, plethysmography measurements and the 6MWT could not be undertaken; this is certainly something worth considering for longitudinal studies in AATD patients. It is important to recognize that we used a cylindrical airway geometry model to estimate MRI  $L_m$  which may not be appropriate in the case of very severe emphysema. Recent work examined the use of three different emphysema modelling approaches and showed good agreement between the cylindrical model and another model which made no geometrical assumptions.<sup>29</sup> This and the fact that we did not constrain internal acinar duct radial parameters suggests that the comparisons made here between COPD and AATD patients are physiologically relevant. In addition to this, these results are in agreement with recent morphomic measurements,<sup>23</sup> taken at 1.5T, using histology and diffusion-weighted MRI which measured S/V ratios of approximately 250 cm<sup>-1</sup> for healthy controls, 100-140 cm<sup>-1</sup> for mild emphysema and 50-55 cm<sup>-1</sup> for severe emphysema. These findings are in good agreement with S/V values measured here in never-smoker (S/V=200±50 cm<sup>-1</sup>), COPD (S/V=110±50 cm<sup>-1</sup>) and AATD subjects (S/V=50±20 cm<sup>-1</sup>). We should also underscore the age difference between the study groups which is a limitation of the study because it was previously established<sup>54</sup> that MRI ADC and  $L_m$  values are age-dependent values. Importantly, the AATD participants we evaluated were significantly younger than the COPD patients, even though lung disease severity based on imaging biomarkers was greater. This suggests that the elevated ADC and  $L_m$  values in the AATD patients were not due to age differences.

An important limitation is the fact that MRI was performed at FRC+1L in all participants (i.e., the lung inflation volume was not normalized across subjects). This is important because lung inflation volume, alveolar inflation and ADC/morphometry values are related. In our study, MRI was performed at FRC+1L in all participants, with coaching by a pulmonary function technologist, to ensure that lung volumes were reproducible within and between participants. This lung volume has been used extensively in the past which allows for comparison with previous studies and this is, in our experience a relatively straightforward maneuver for patients with respiratory disease. We note however, that for

NS-2 and NS-5, the FRC+1L volume was very similar (FRC+1L = 3.8±0.2L) and there was no significant correlation between L<sub>m</sub> and TLC (p=.7) and L<sub>m</sub> and FRC+1L (p=.9).

This present study builds upon previous MRI studies in AATD patients<sup>25-28</sup> that evaluated ADC measurements and their changes over relatively short periods of time. Previous work in COPD patients<sup>50</sup> and healthy volunteers<sup>39,51</sup> provides a foundation for the current study that extends the two b-value ADC approach with a single breath whole lung multiple b-value morphometry approach.<sup>29</sup> MRI provides similar and complementary information to CT with the advantage of being free of ionizing radiation, which is important for AATD patients who are diagnosed at relatively young ages. These patients have the opportunity to undergo augmentation therapy; MRI biomarkers that provide sensitive measurements of airspace enlargement can be considered for these treatment studies and longitudinal evaluations. MRI also offers novel structure-function biomarkers including measurements of parenchyma microstructure that correlate with histological samples.<sup>21,23,24</sup> Moreover, as we transition to inhaled <sup>129</sup>Xe gas as contrast,<sup>16</sup> it is important to note that dissolved-phase <sup>129</sup>Xe MRI may be employed to simultaneously estimate ventilation, perfusion<sup>52</sup> and surrogate measurements of DL<sub>CO</sub>.<sup>53</sup> This information may be very helpful in studies that evaluate augmentation therapy and other AATD treatments for which direct evidence of efficacy<sup>3,4</sup> has been difficult to ascertain.

In summary, MRI biomarkers of emphysema were significantly different in AATD subjects as compared to age-matched never-smokers and older ex-smokers with smoking-related emphysema. Importantly, the significantly different and abnormal L<sub>m</sub> values in AATD patients, who were not significantly different from COPD patients with respect to pulmonary function tests and CT emphysema measurements, reveals the sensitivity of MRI emphysema measurements in AATD patients for whom lifelong monitoring is required.

## 2.5 References

- (1) Laurell C-B, Eriksson S. The electrophoretic  $\alpha_1$ -globulin pattern of serum in  $\alpha_1$ -antitrypsin deficiency. *Scand J Clin Lab Invest.* 1963; 15(2):132-140.
- (2) Stoller JK, Aboussouan LS. A review of  $\alpha_1$ -antitrypsin deficiency. *Am J Respir Crit Care Med.* 2012; 185(3):246-259.



- (3) Marciniuk D, Hernandez P, Balter M, et al. Alpha-1 antitrypsin deficiency targeted testing and augmentation therapy: A Canadian Thoracic Society clinical practice guideline. *Can Respir J*. 2012; 19(2):109-116.
- (4) Chapman KR, Burdon JG, Piitulainen E, et al. Intravenous augmentation treatment and lung density in severe alpha1 antitrypsin deficiency (RAPID): a randomised, double-blind, placebo-controlled trial. *Lancet*. 2015; 386(9991):360-368.
- (5) Crystal RG. Augmentation treatment for alpha1 antitrypsin deficiency. *Lancet*. 2015; 386(9991):318-320.
- (6) Yusa K, Rashid ST, Strick-Marchand H, et al. Targeted gene correction of [agr]1-antitrypsin deficiency in induced pluripotent stem cells. *Nature*. 2011; 478(7369):391-394.
- (7) Rashid ST, Lomas DA. Stem cell-based therapy for  $\alpha(1)$ -antitrypsin deficiency. *Stem Cell Res Ther*. 2012; 3(1):1.
- (8) Seersholm N, Wencker M, Banik N, et al. Does alpha1-antitrypsin augmentation therapy slow the annual decline in FEV1 in patients with severe hereditary alpha1-antitrypsin deficiency? Wissenschaftliche Arbeitsgemeinschaft zur Therapie von Lungenerkrankungen (WATL) alpha1-AT study group. *Eur Respir J*. 1997; 10(10):2260-2263.
- (9) Vreim C, Wu M, Crystal R, et al. Survival and FEV1 decline in individuals with severe deficiency of alpha (1)-antitrypsin. *Am J Respir Crit Care Med*. 1998; 158(1):49-59.
- (10) Wencker M, Fuhrmann B, Banik N, Konietzko N. Longitudinal Follow-up of Patients With  $\alpha 1$ -Protease Inhibitor Deficiency Before and During Therapy With IV  $\alpha 1$ -Protease Inhibitor\*. *Chest*. 2001; 119(3):737-744.
- (11) Hathaway EH, Tashkin D, Simmons MS. Intraindividual Variability in Serial Measurements of OLeo and Alveolar Volume over One Year in Eight Healthy Subjects Using Three Independent Measuring Systems. *Am Rev Respir Dis*. 1989; 140:1818-1822.
- (12) Morrison NJ, Abboud RT, Ramadan F, et al. Comparison of single breath carbon monoxide diffusing capacity and pressure-volume curves in detecting emphysema. *Am Rev Respir Dis*. 1989; 139(5):1179-1187.
- (13) Gould GA, Redpath AT, Ryan M, et al. Lung CT density correlates with measurements of airflow limitation and the diffusing capacity. *Eur Respir J*. 1991; 4(2):141-146.
- (14) Dawkins PA, Dowson LJ, Guest PJ, Stockley RA. Predictors of mortality in alpha1-antitrypsin deficiency. *Thorax*. 2003; 58(12):1020-1026.
- (15) Saam BT, Yablonskiy DA, Kodibagkar VD, et al. MR imaging of diffusion of 3He gas in healthy and diseased lungs. *Magn Reson Med*. 2000; 44(2):174-179.

- (16) Kim W, Eidelman DH, Izquierdo JL, Ghezzi H, Saetta MP, Cosio MG. Centrilobular and panlobular emphysema in smokers. *Am Rev Respir Dis.* 1991; 144:1385-1390.
- (17) Yablonskiy DA, Sukstanskii AL, Leawoods JC, et al. Quantitative in vivo assessment of lung microstructure at the alveolar level with hyperpolarized <sup>3</sup>He diffusion MRI. *Proc Natl Acad Sci U S A.* 2002; 99(5):3111-3116.
- (18) Kirby M, Ouriadov A, Svenningsen S, et al. Hyperpolarized <sup>3</sup>He and <sup>129</sup>Xe magnetic resonance imaging apparent diffusion coefficients: physiological relevance in older never - and ex - smokers. *Physiol Rep.* 2014; 2(7):e12068.
- (19) Chan HF, Stewart NJ, Parra-Robles J, Collier GJ, Wild JM. Whole lung morphometry with 3D multiple b-value hyperpolarized gas MRI and compressed sensing. *Magn Reson Med.* 2016:<http://dx.doi.org/10.1002/mrm.26279>.
- (20) Weibel E. Geometry and Dimensions of Airways of Conductive and Transitory Zones. *Morphometry of the Human Lung*; Springer Berlin Heidelberg; 1963; 110-135.
- (21) Woods JC, Choong CK, Yablonskiy DA, et al. Hyperpolarized <sup>3</sup>He diffusion MRI and histology in pulmonary emphysema. *Magn Reson Med.* 2006; 56(6):1293-1300.
- (22) Tanoli TS, Woods JC, Conradi MS, et al. In vivo lung morphometry with hyperpolarized <sup>3</sup>He diffusion MRI in canines with induced emphysema: disease progression and comparison with computed tomography. *J Appl Physiol.* 2007; 102(1):477-484.
- (23) Yablonskiy DA, Sukstanskii AL, Woods JC, et al. Quantification of lung microstructure with hyperpolarized <sup>3</sup>He diffusion MRI. *J Appl Physiol.* 2009; 107(4):1258-1265.
- (24) Thomen RP, Quirk JD, Roach D, et al. Direct comparison of Xe diffusion measurements with quantitative histology in human lungs. *Magn Reson Med.* 2016:<http://dx.doi.org/10.1002/mrm.26120>.
- (25) Diaz S, Casselbrant I, Piitulainen E, et al. Progression of Emphysema in a 12-month Hyperpolarized <sup>3</sup>He-MRI Study: Lacunarity Analysis Provided a More Sensitive Measure than Standard ADC Analysis. *Acad Radiol.* 2009; 16(6):700-707.
- (26) Stavngaard T, Sogaard LV, Batz M, Schreiber L, Dirksen A. Progression of emphysema evaluated by MRI using hyperpolarized <sup>3</sup>He (hp <sup>3</sup>He) measurements in patients with alpha-1-antitrypsin (a1at) deficiency compared with CT and lung function tests. *Acta Radiol.* 2009; 50(9):1019-1026.
- (27) Van Beek E, Dahmen A, Stavngaard T, et al. Hyperpolarised <sup>3</sup>He MRI versus HRCT in COPD and normal volunteers: PHIL trial. *Eur Respir J.* 2009; 34(6):1311-1321.

- (28) Diaz S, Casselbrant I, Piitulainen E, et al. Hyperpolarized  $^3\text{He}$  apparent diffusion coefficient MRI of the lung: reproducibility and volume dependency in healthy volunteers and patients with emphysema. *J Magn Reson Imaging*. 2008; 27(4):763-770.
- (29) Ouriadov A, Lessard E, Sheikh K, Parraga G. Pulmonary MRI morphometry modeling of airspace enlargement in chronic obstructive pulmonary disease and  $\alpha$ -1 antitrypsin deficiency. *Magn Reson Med*. 2017.
- (30) Gevenois PA, De Vuyst P, de Maertelaer V, et al. Comparison of computed density and microscopic morphometry in pulmonary emphysema. *Am J Respir Crit Care Med*. 1996; 154(1):187-192.
- (31) Miller MR, Hankinson J, Brusasco V, et al. Standardisation of spirometry. *Eur Respir J*. 2005; 26(2):319-338.
- (32) Jones PW, Quirk FH, Baveystock CM, Littlejohns P. A self-complete measure of health status for chronic airflow limitation: the St. George's Respiratory Questionnaire. *Am Rev Respir Dis*. 1992; 145(6):1321-1327.
- (33) Enright PL. The six-minute walk test. *Respir Care*. 2003; 48(8):783-785.
- (34) Parraga G, Ouriadov A, Evans A, et al. Hyperpolarized  $^3\text{He}$  ventilation defects and apparent diffusion coefficients in chronic obstructive pulmonary disease: preliminary results at 3.0 Tesla. *Invest Radiol*. 2007; 42(6):384-391.
- (35) Miller G, Altes T, Brookeman J, De Lange E, Mugler Iii J. Hyperpolarized  $^3\text{He}$  lung ventilation imaging with B<sub>1</sub>-inhomogeneity correction in a single breath-hold scan. *MAGMA*. 2004; 16(5):218-226.
- (36) Ouriadov AV, Lam WW, Santyr GE. Rapid 3-D mapping of hyperpolarized  $^3\text{He}$  spin-lattice relaxation times using variable flip angle gradient echo imaging with application to alveolar oxygen partial pressure measurement in rat lungs. *MAGMA*. 2009; 22(5):309-318.
- (37) Kirby M, Heydarian M, Svenningsen S, et al. Hyperpolarized  $^3\text{He}$  magnetic resonance functional imaging semiautomated segmentation. *Acad Radiol*. 2012; 19(2):141-152.
- (38) Kirby M, Heydarian M, Wheatley A, McCormack DG, Parraga G. Evaluating bronchodilator effects in chronic obstructive pulmonary disease using diffusion-weighted hyperpolarized helium-3 magnetic resonance imaging. *J Appl Physiol*. 2012; 112(4):651-657.
- (39) Paulin GA, Ouriadov A, Lessard E, Sheikh K, McCormack DG, Parraga G. Noninvasive quantification of alveolar morphometry in elderly never- and ex-smokers. *Physiol Rep*. 2015; 3(10):e12583.

- (40) Sukstanskii AL, Yablonskiy DA. In vivo lung morphometry with hyperpolarized  $^3\text{He}$  diffusion MRI: theoretical background. *J Magn Reson.* 2008; 190(2):200-210.
- (41) Hajari AJ, Yablonskiy DA, Quirk JD, et al. Imaging alveolar-duct geometry during expiration via  $^3\text{He}$  lung morphometry. *J Appl Physiol.* 2011; 110(5):1448-1454.
- (42) Yablonskiy DA, Sukstanskii AL, Conradi MS. Commentary on "The influence of lung airways branching structure and diffusion time on measurements and models of short-range  $^3\text{He}$  gas MR diffusion". *J Magn Reson.* 2014; 239:139-142.
- (43) Needham M, Stockley R.  $\alpha$ 1-Antitrypsin deficiency• 3: Clinical manifestations and natural history. *Thorax.* 2004; 59(5):441-445.
- (44) Mishima M, Hirai T, Itoh H, et al. Complexity of terminal airspace geometry assessed by lung computed tomography in normal subjects and patients with chronic obstructive pulmonary disease. *Proc Natl Acad Sci U S A.* 1999; 96(16):8829-8834.
- (45) Capaldi DP, Zha N, Guo F, et al. Pulmonary imaging biomarkers of gas trapping and emphysema in COPD:  $^3\text{He}$  MR imaging and CT parametric response maps. *Radiology.* 2016; 279(2):597-608.
- (46) Kirby M, Pike D, Coxson HO, McCormack DG, Parraga G. Hyperpolarized  $^3\text{He}$  ventilation defects used to predict pulmonary exacerbations in mild to moderate chronic obstructive pulmonary disease. *Radiology.* 2014; 273(3):887-896.
- (47) Diaz AA, Valim C, Yamashiro T, et al. Airway count and emphysema assessed by chest CT imaging predicts clinical outcome in smokers. *Chest.* 2010; 138(4):880-887.
- (48) Parr DG, Stoel BC, Stolk J, Stockley RA. Pattern of emphysema distribution in  $\alpha$ 1-antitrypsin deficiency influences lung function impairment. *Am J Respir Crit Care Med.* 2004; 170(11):1172-1178.
- (49) Kirby M, Owrangi A, Svenningsen S, et al. On the role of abnormal DLCO in ex-smokers without airflow limitation: symptoms, exercise capacity and hyperpolarised helium-3 MRI. *Thorax.* 2013:thoraxjnl-2012-203108.
- (50) Lessard E, Ouriadov A, Capaldi DP, McCormack DG, Parraga G. Novel Biomarkers Of Lung Parenchyma Destruction And Emphysema Progression In COPD Using Inhaled Gas MRI Morphometry. *Am J Respir Crit Care Med*; 2016; 193:A7526 [Abstract].
- (51) Morbach AE, Gast KK, Schmiedeskamp J, et al. Diffusion-weighted MRI of the lung with hyperpolarized helium-3: a study of reproducibility. *J Magn Reson Imaging.* 2005; 21(6):765-774.

- (52) Mathew L, Evans A, Ouriadov A, et al. Hyperpolarized  $^3\text{He}$  magnetic resonance imaging of chronic obstructive pulmonary disease: reproducibility at 3.0 Tesla. *Acad Radiol.* 2008; 15(10):1298-1311.
- (53) Quirk JD, Chang YV, Yablonskiy DA. In vivo lung morphometry with hyperpolarized ( $^3\text{He}$ ) diffusion MRI: reproducibility and the role of diffusion-sensitizing gradient direction. *Magn Reson Med.* 2015; 73(3):1252-1257.
- (54) Quirk JD, Sukstanskii AL, Woods JC, et al. Experimental evidence of age-related adaptive changes in human acinar airways. *J Appl Physiol.* 2016; 120(2):159-165.
- (55) Quirk JD, Lutey BA, Gierada DS, et al. In Vivo Detection of Acinar Microstructural Changes in Early Emphysema with  $^3\text{He}$  Lung Morphometry. *Radiology.* 2011; 260(3):866-874.
- (56) Kaushik SS, Freeman MS, Cleveland ZI, et al. Probing the regional distribution of pulmonary gas exchange through single-breath gas-and dissolved-phase  $^{129}\text{Xe}$  MR imaging. *J Appl Physiol.* 2013; 115(6):850-860.
- (57) Fairbanks KD, Tavill AS. Liver disease in alpha 1-antitrypsin deficiency: a review. *Am J Gastroenterol.* 2008; 103(8):2136-2141.

## 3 Chapter 3: Conclusions and Future Directions

### 3.1 Overview and Research Questions

This thesis sought to provide measurements of pulmonary airspace enlargement using diffusion-weighted MRI in COPD and AATD. This is crucial as quantification of lung structure can be considered the gold standard in evaluation of response to treatment in COPD.<sup>1</sup> COPD is a disease that has tremendous costs both economically and socially in Canada<sup>2</sup> and worldwide.<sup>3</sup>

### 3.2 Summary and Conclusions

In this thesis, I examined a sample of patients with AATD. I demonstrated that, by using a multiple-b value diffusion-weighted MRI approach, I could obtain similar, and complimentary, information to CT; this finding is important in the case of AATD where disease begins at a young age making longitudinal evaluation of disease using CT unattractive due to cumulative dose effects. I compared these patients to age-matched healthy never-smokers and the AATD subjects were significantly worse as measured by both CT (LAC and RA<sub>950</sub>) and <sup>3</sup>He diffusion MRI (VDP, ADC and morphometry). In addition, I compared these AATD patients to a group of ex-smokers with smoking related emphysema. These groups showed no differences in spirometry, CT measurements, ventilation measurements or exercise capabilities but the AATD group was statistically worse in terms of perceived quality of life, whole lung and basal ADC, and morphometry values (whole lung, apical and basal). These results showed that using a small sample population it is possible to elucidate differences in disease severity by using diffusion-weighted MRI. Ultimately, this approach may provide a method of performing smaller clinical trials examining treatment efficacy in AATD drug development.

In summary, I have 1) examined a patient population who would greatly benefit from inhaled noble-gas morphometry as a sensitive measurement of disease severity, 2) demonstrated that whole lung multiple b-value measurements of airspace enlargement are feasible in this population and 3) demonstrated that this technique can differentiate between

smoking-related disease and AATD-related disease even in the absence of spirometry or CT differences.

### 3.3 Limitations

Study specific limitations are discussed in detail in **Chapter 2** but the most important limitations from **Chapter 2** and a few major limitations will be discussed in more detail here.

In **Chapter 2** we explored a small sample of AATD patients (n=8) and observed significantly elevated morphometry values of airspace enlargement. These are elevated as compared to COPD ex-smokers and age-matched elderly never-smokers. The AATD subjects showed no difference between the COPD ex-smokers as visualized using CT or using standard clinical airflow measurements.

Outside of the study specific limitations, there exist limitations inherent to the inhaled noble-gas morphometry method. Inhaled noble-gas morphometry measurements are inherently reliant on gas dispersion throughout the lungs. Essentially, in regions of ventilation defect, morphometry measurements cannot be acquired. When reporting a whole lung mean value, this will skew the measurement towards the healthy lung tissue (regions which are ventilated). Furthermore, this excludes fractions of the lung for quantitative evaluation, and unfortunately non-ventilated regions cannot distinguish between emphysematous destruction, mucus clogged airways or other reasons for lack of ventilation.

Another major limitation of the ADC technique is the intrinsic variation in ADC measurements that depend on gradient timing parameters. The temporal profile of the applied bipolar diffusion gradients affects the ADC measurement and as such it is important to keep this consistent between scans.<sup>4,5</sup> Furthermore there is the effect of field strength on ADC measurements.<sup>4</sup> Briefly, in previous work the authors observed significantly elevated ADC measurements obtained in the same subjects (n=5, healthy volunteers) at 3T versus 1.5T. The authors concluded this difference was due to susceptibility-induced field inhomogeneities. Although, these differences could be

accounted for by differences in scanner manufacturers (Philips 3T and GE 1.5T). However, this is still important to keep in mind when comparing measurements across centres as a difference in obtained ADC may be due to a difference in field strength or possibly scanner manufacturer. Other factors, such as the spatial profile of the magnetic field, surface relaxation and surface permeability, also have an effect on the ADC measured.<sup>5</sup>

Perhaps the most important limitation of this thesis work is the availability and cost of  $^3\text{He}$  and limited access to polarization equipment. This can be partially resolved through transition to  $^{129}\text{Xe}$  which is more cost effective and naturally abundant. However, until recently similar levels of polarization could not be achieved with  $^{129}\text{Xe}$  as could be achieved with  $^3\text{He}$ .  $^{129}\text{Xe}$  still needs to be polarized prior to use but can reach required polarization much quicker (~45 minutes) versus  $^3\text{He}$  (~18 hours) which makes it attractive for performing serial scans in a single day. However,  $^{129}\text{Xe}$  that has been polarized and prepared for administration must be used as it now resides outside of the gas cell.  $^3\text{He}$  however does not exit the gas cell until immediately before administration meaning in the event of scan cancelation or failures up until the moment of administration  $^3\text{He}$  can still be recovered and used later whereas  $^{129}\text{Xe}$  will be wasted, or at best needs to be recycled.

## 3.4 Future Directions

### 3.4.1 Overcoming Issues Related to Gas Dispersion

A method of overcoming gas dispersion issues with regards to measuring tissue microstructure has been explored using modelled Carr-Purcell-Meiboom-Gill (CPMG) inter-echo time  $R_2$  dispersion<sup>6</sup> unfortunately this method has yet to transition into *in vivo* measurements. Briefly, in this work the authors tested an *in silico* model of alveoli as spherical airspaces and derived equations for the relaxation rate  $R_2$ , the transverse relaxation rate. They tested their model against deflated rat lungs and demonstrated good agreement between the mean alveolar radius as measured using this technique ( $31.5 \pm 13 \mu\text{m}$ ) and literature ( $34 \mu\text{m}$ ).



### 3.4.2 Accelerated Imaging

Diffusion-weighted MRI with multiple-b values (5 values) may require as much as 16 seconds acquiring 7 slices. With parallel imaging or compressed sensing, the scan speed can be greatly increased and the possibility of greater number of slices (>14) can be achieved. With this there would no longer be a requirement of taking a separate static ventilation scan to obtain VDP measurements. This would in theory halve the required volume of gas used to obtain a full set of information that MRI can provide (VDP, ADC, morphometry). This is especially important both in a clinical setting and a research setting as the cost of  $^3\text{He}$  continues to rise due to its natural scarcity. Another possible benefit would be towards isotropic voxel sizes. Currently  $3.125 \times 3.125 \times 30 \text{ mm}^3$  are common for diffusion-weighted scans, and  $3.125 \times 3.125 \times 15 \text{ mm}^3$  are common for static ventilation scans. With a large increase in scan speed, smaller voxels would be possible. Preliminary work has been done with acceleration factors up to x10 with only some lost details as compared to no acceleration.<sup>7</sup>

Implementation of parallel imaging, using a multi-channel receive array, would allow an increase in scan speed. However, it comes with limitations in reduced FOV and aliasing artifacts. Using the known spatial information of the coils the resulting images are “unfolded” and the original image is reconstructed. Preliminary work has been performed<sup>8</sup> using generalized autocalibrating partially parallel acquisitions (GRAPPA) and an 8-channel receive coil, which demonstrated that lung morphometry can be calculated using parallel imaging without significant differences in measurements. They conclude that even though the work was performed using  $^3\text{He}$  that it could be generalized to  $^{129}\text{Xe}$ . This in turn makes this technique more clinically translatable.

### 3.4.3 The Transition to $^{129}\text{Xe}$

Much of the work in noble-gas lung morphometry has been done using  $^3\text{He}$  due to its high gyromagnetic ratio and achievable polarization levels. However, with the inevitable transition from  $^3\text{He}$  to  $^{129}\text{Xe}$  due to the lower cost and greater natural abundance of  $^{129}\text{Xe}$ , it is important to ensure that methods can also be translated. In our lab<sup>9</sup> we have compared three different acinar duct models relying on  $^3\text{He}$  diffusion. The cylindrical model used in

this thesis already has a theoretical formulation for the use of  $^{129}\text{Xe}$  and can be readily translated.<sup>10</sup> Another geometrical model assuming spherical symmetry was explored which is based on varying the diffusion time as opposed to b-value during the scan and can be readily transitioned to use with  $^{129}\text{Xe}$ . The third model, the stretched exponential model, is without geometrical assumptions, nor assumptions regarding gas diffusivity and due to this would also be translatable to  $^{129}\text{Xe}$ . These considerations are important if this method is to be used to longitudinally evaluate patients with AATD.

Outside of technical challenges, there is still much work to be done identifying potential biomarkers of disease using diffusion-weighted MRI in the lung.

#### 3.4.4 Functional Diffusion Maps of the Lungs

There has been work in other organs, specifically in the brain examining the change in ADC measurements in an imaging voxel across periods of time.<sup>11</sup> Functional Diffusion Maps (FDM), are co-registered ADC maps that stratify regions of the brain into three distinct categories, i.e., regions which have increased ADC, unchanged ADC or decreased ADC. FDM has been examined as an early marker of biologic outcome and shows promise as a tool to predict treatment efficacy early in the drug development process.<sup>12</sup> Although much of this work has been performed in analysis of the brain, FDM can be applied in a similar fashion as a potential lung disease biomarker. To use FDM for lung disease, ADC images are taken at time points  $t_1$  and  $t_2$  ( $t_2 > t_1$ ). These images are registered together using an affine transformation<sup>13</sup> using the  $b = 0$  s/cm<sup>2</sup> slice to ensure the highest signal image is used in the registration. Unlike in traditional brain FDM, an imaging voxel within the lung can be categorized into one of five categories: 1) increased ADC, 2) decreased ADC, 3) no change in ADC, 4) lost ventilation (i.e signal void at  $t_2$  where there was signal at  $t_1$ ) and 5) gained ventilation (i.e signal at  $t_2$  where there was a signal void at  $t_1$ ). In order to determine whether a voxel has increased (or decreased) in ADC at  $t_2$  versus  $t_1$ , a threshold (T) must be determined to categorize a change as significant. A voxel is categorized as no change in ADC if  $|\Delta\text{ADC}| < T$ . As a first step in determining T, the variability in ADC measurements must be determined. Previous work<sup>14</sup> has examined same-day rescan and 7-day rescan and has demonstrated a coefficient of variation (COV) and mean ADC for

never-smokers, mild-moderate COPD and severe COPD. Using the COV and mean ADC for each subgroup, a variability of approximately  $0.01 \text{ cm}^2/\text{s}$  applies across all groups. As a preliminary step, I defined a threshold of  $T = 0.01 \text{ cm}^2/\text{s}$  as a significant deviation from the  $t_1$  scan. **Figure 3-1** shows a sample workflow for analysis of an AATD subject at two time points.

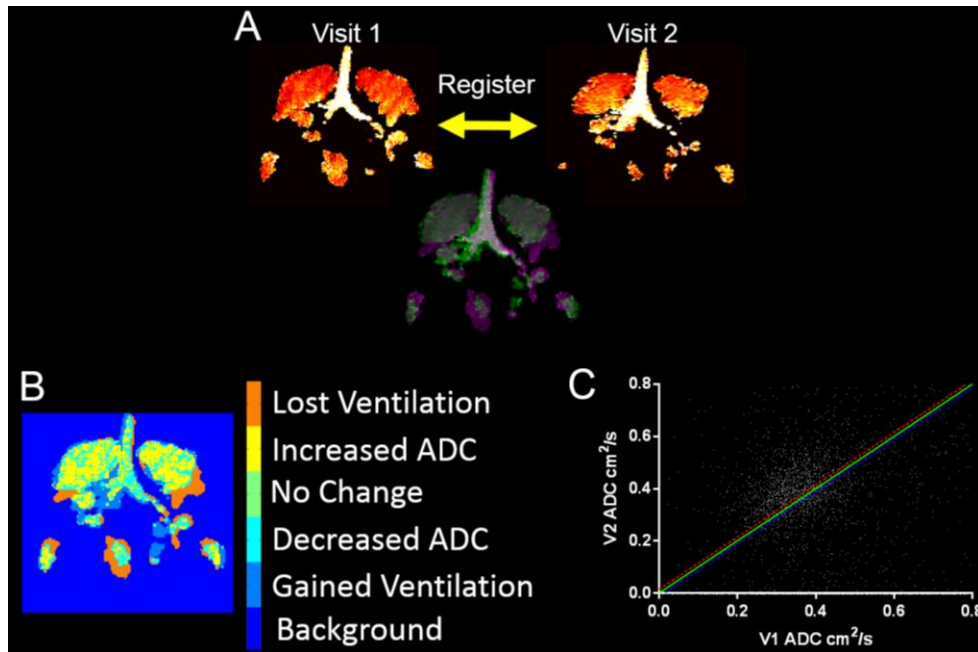


**Figure 3-1: Functional Diffusion Map Workflow**

A) Two visit ADC maps are co-registered

B) Functional diffusion map is generated and clustered into 5 distinct non background regions

C) A plot of V1 vs V2 ADC with points above the red line showing regions of increased ADC and points below the blue line showing regions of worse ADC. Green line shows line of identity

In order to evaluate the effect of a landmark based affine transformation and user variability on these five distinct regions, a single subject was evaluated five times each day for five days. The coefficient of variation across both same-day and five day variability was determined to be 1%, indicating little variation between trials, this is important for implementation of this technique. Future work should be aimed at examining large patient databases with multi-visit ADC measurements and evaluating relationships between clinical outcomes and FDM measurements. Although the focus here has been on 2-visit ADC maps, it would be possible to extend this to n-visit maps and examine the longitudinal

change in ADC either as a voxel-wise slope or possibly through another method of analysis. With the focus of this thesis on multiple-b measurements of airspace enlargement, it would be simple to extend FDM to  $L_m$  maps or any other morphometry measurement acquired using the morphomic technique.

### 3.4.5 Longitudinal Evaluation of AATD

This thesis examined AATD disease cross-sectionally. To build upon this cross-sectional evaluation, a longitudinal study evaluating disease progression over longer periods of time should be performed to examine the change in lung function as measured by standard clinical tools and by using hyperpolarized noble-gas MRI. A small, preliminary evaluation of a single AATD subject (AATD-1 from this thesis) was performed over the course of approximately five years (**Figure 3-2**).

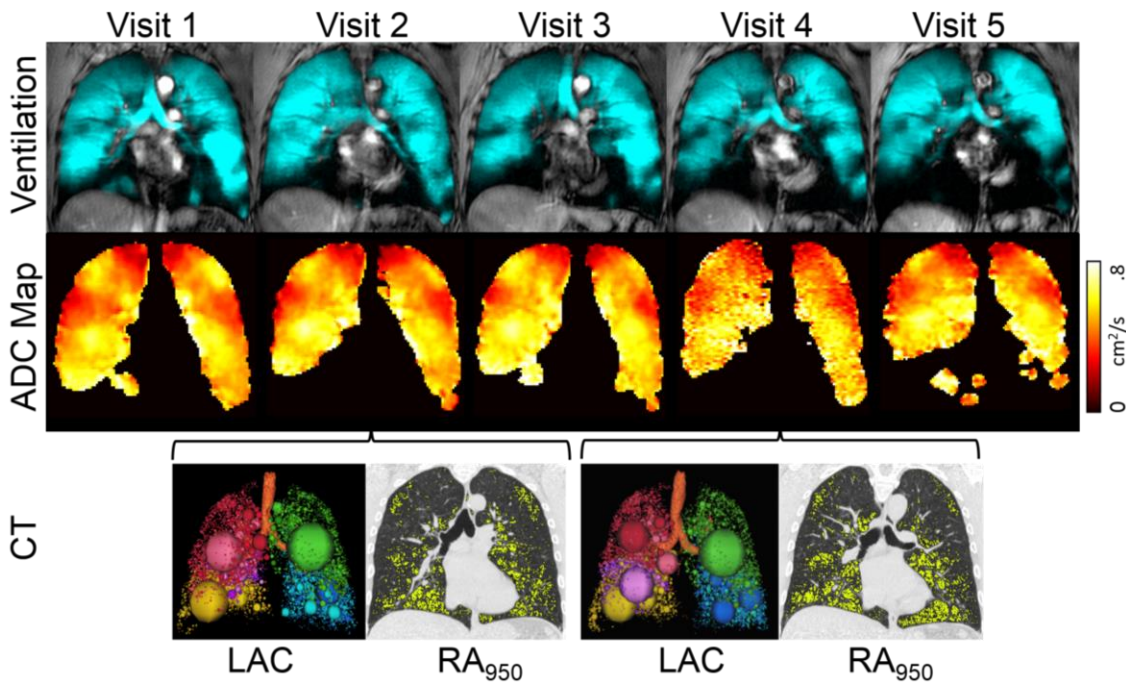


**Figure 3-2: Longitudinal Evaluation of AATD**

As shown in **Figure 3-2** the subject has lost ventilation over time (primarily in the lower lobes as to be expected in AATD related disease) and shows an increase in both ADC and  $RA_{950}$  qualitatively located in the basal portion of the lungs. Although this analysis was performed only a single subject it provides motivation for larger longitudinal studies in

AATD, with the possibility of examining subjects with and without augmentation therapy. In a continuation study currently undergoing in our lab, subjects with AATD are being recruited and will be scanned longitudinally (1-3 years follow-up) to examine their lung function decline as measured using both spirometry and imaging techniques such as CT and hyperpolarized MRI. Furthermore, by acquiring  $^{129}\text{Xe}$  images in this population, the techniques used and information gained from this study will be one step closer to clinical translation.

### 3.5 Significance and Impact

Alpha-1 antitrypsin deficiency results in early onset chronic obstructive pulmonary disease and there is no available cure. Current therapies rely on slowing disease progression. Longitudinal evaluation of this population is done with nonspecific airflow measurements and frequent CT scans with the burden of ionizing radiation. Clinical trial endpoints unfortunately still rely on these methods. Hyperpolarized noble-gas diffusion-weighted MRI, in particular  $L_m$ , provides an opportunity to fill the role of a clinical trial endpoint and provide a measurement of treatment response that is sensitive to both disease progression and airspace enlargement. Diffusion-weighted MRI combines the ability to obtain ventilation defect percentage and measurements of tissue microstructure obtainable within a single breath-hold without the use of ionizing radiation, making it an attractive clinical trial endpoint to gauge treatment efficacy. Using a smaller sample than currently used in clinical trials, treatment efficacy can be evaluated quantitatively using multiple-b diffusion MRI and can impact the time and cost associated with development of novel treatments for AATD.

### 3.6 References

- (1) Hsia, C. C., Hyde, D. M., Ochs, M. & Weibel, E. R. An official research policy statement of the American Thoracic Society/European Respiratory Society: standards for quantitative assessment of lung structure. *American journal of respiratory and critical care medicine* 2010; 181: 394-418.
- (2) Chapman, K., Bourbeau, J. & Rance, L. The burden of COPD in Canada: results from the Confronting COPD survey. *Respiratory Medicine* 2003; 97: S23-S31.

- (3) Global Alliance against Chronic Respiratory Diseases. World Health Organization Fact Sheet N 315, <<http://www.who.int/mediacentre/factsheets/fs315/en/>> (2012)
- (4) Parra-Robles, J. *et al.* The influence of field strength on the apparent diffusion coefficient of  $^3\text{He}$  gas in human lungs. *Magnetic resonance in medicine* 2012; 67: 322-325.
- (5) Grebenkov, D. S. Use, misuse, and abuse of apparent diffusion coefficients. *Concepts in Magnetic Resonance Part A* 2010; 36: 24-35.
- (6) Kurz, F. T. *et al.* Microstructural analysis of peripheral lung tissue through CPMG inter-echo time  $R_2$  dispersion. *PloS one* 2015; 10: e0141894.
- (7) Abascal, J. F., Desco, M. & Parra-Robles, J. Incorporation of prior knowledge of the signal behavior into the reconstruction to accelerate the acquisition of MR diffusion data. *arXiv preprint arXiv:1702.02743* 2017.
- (8) Chang, Y. V., Quirk, J. D. & Yablonskiy, D. A. In vivo lung morphometry with accelerated hyperpolarized ( $^3\text{He}$ ) diffusion MRI: a preliminary study. *Magn Reson Med* 2015; 73: 1609-1614.
- (9) Ouriadov, A., Lessard, E., Sheikh, K. & Parraga, G. Pulmonary MRI morphometry modeling of airspace enlargement in chronic obstructive pulmonary disease and alpha-1 antitrypsin deficiency. *Magnetic Resonance in Medicine* 2017.
- (10) Sukstanskii, A. L. & Yablonskiy, D. A. Lung morphometry with hyperpolarized  $^{129}\text{Xe}$ : theoretical background. *Magn Reson Med* 2012; 67: 856-866.
- (11) Moffat, B. A. *et al.* Functional diffusion map: a noninvasive MRI biomarker for early stratification of clinical brain tumor response. *Proceedings of the National Academy of Sciences of the United States of America* 2005; 102: 5524-5529.
- (12) Moffat, B. A. *et al.* The functional diffusion map: an imaging biomarker for the early prediction of cancer treatment outcome. *Neoplasia* 2006; 8: 259-267.
- (13) Kirby, M. *et al.* Hyperpolarized  $^3\text{He}$  magnetic resonance functional imaging semiautomated segmentation. *Academic radiology* 2012; 19: 141-152.
- (14) Parraga, G. *et al.* Hyperpolarized  $^3\text{He}$  ventilation defects and apparent diffusion coefficients in chronic obstructive pulmonary disease: preliminary results at 3.0 Tesla. *Invest Radiol* 2007; 42: 384-391.

## 4 Appendix

### Appendix A - Permission for Reproduction of Scientific Articles

Dear Eric J. Lessard:

The Radiological Society of North America (RSNA<sup>\*</sup>) is pleased to grant you permission to reproduce the following figures in print and electronic formats for educational, non-profit use in your dissertation/thesis, provided you give full credit to the authors of the original publication.


Figures 1a, 1b, 2a, 2b

Watz H, Breithecker A, Rau W S, et al. Micro-CT of the human lung: Imaging of alveoli and virtual endoscopy of an alveolar duct in a normal lung and in a lung with centrilobular emphysema—Initial observations. *Radiology* 2005;236:1053-1058.

This permission is a one-time, non-exclusive grant for English-language use and is exclusively limited to the usage stated and underlined above. The requestor guarantees to reproduce the material as originally published. Permission is granted under the condition that a full credit line is prominently placed (i.e. author name(s), journal name, copyright year, volume #, inclusive pages and copyright holder).

This permission becomes effective upon receipt of this signed contract. Please sign a copy of this agreement, return a signed copy to me and retain a copy for your files. Thank you for your interest in our publication.

## Appendix B - Health Science Research Ethics Board Approval Notices

	<b>Use of Human Subjects - Ethics Approval Notice</b>
<b>Principal Investigator:</b> Dr. G. Parraga	<b>Review Level:</b> Full Board
<b>Review Number:</b> 17396	<b>Approved Local # of Participants:</b> 180
<b>Review Date:</b> September 14, 2010	
<b>Protocol Title:</b> Longitudinal 3He Magnetic Resonance Imaging of Health Lung	
<b>Department and Institution:</b> Imaging, Robarts Research Institute	
<b>Sponsor:</b> CIHR-CANADIAN INSTITUTE OF HEALTH RESEARCH	
<b>Ethics Approval Date:</b> November 09, 2010	<b>Expiry Date:</b> September 30, 2014
<b>Documents Reviewed and Approved:</b> UWO Protocol (including instruments noted in Section 8.1), Letter of Information and Consent Form dated Sept. 27, 2010 version 2, and Advertisement.	
<b>Documents Received for Information:</b> Clinical Study Protocol Version #1 27 August 2010; IB NC100182-Inhalation (Hyperpolarised 3HE) 6th edition 09 Sep 05; NC1000182 IB April 7, 2009; Product Monograph Ventolin HFA	

This is to notify you that The University of Western Ontario Research Ethics Board for Health Sciences Research Involving Human Subjects (HSREB) which is organized and operates according to the Tri-Council Policy Statement: Ethical Conduct of Research Involving Humans and the Health Canada/ICH Good Clinical Practice Practices: Consolidated Guidelines; and the applicable laws and regulations of Ontario has reviewed and granted approval to the above referenced study on the approval date noted above. The membership of this REB also complies with the membership requirements for REB's as defined in Division 5 of the Food and Drug Regulations.

The ethics approval for this study shall remain valid until the expiry date noted above assuming timely and acceptable responses to the HSREB's periodic requests for surveillance and monitoring information. If you require an updated approval notice prior to that time you must request it using the UWO Updated Approval Request Form.

During the course of the research, no deviations from, or changes to, the protocol or consent form may be initiated without prior written approval from the HSREB except when necessary to eliminate immediate hazards to the subject or when the change(s) involve only logistical or administrative aspects of the study (e.g. change of monitor, telephone number). Expedited review of minor change(s) in ongoing studies will be considered. Subjects must receive a copy of the signed information/consent documentation.

Investigators must promptly also report to the HSREB:

- changes increasing the risk to the participant(s) and/or affecting significantly the conduct of the study;
- all adverse and unexpected experiences or events that are both serious and unexpected;
- new information that may adversely affect the safety of the subjects or the conduct of the study.

If these changes/adverse events require a change to the information/consent documentation, and/or recruitment advertisement, the newly revised information/consent documentation, and/or advertisement, must be submitted to this office for approval.

Members of the HSREB who are named as investigators in research studies, or declare a conflict of interest, do not participate in discussion related to, nor vote on, such studies when they are presented to the HSREB.





Western University Health Science Research Ethics Board  
HSREB Amendment Approval Notice

Principal Investigator: Dr. Grace Parraga  
Department & Institution: Schulich School of Medicine and Dentistry/Imaging, Roberts Research Institute

HSREB File Number: 7320  
Study Title: Longitudinal 31e Magnetic Resonance Imaging of Healthy Lung (REB #17396)  
Sponsor: Canadian Institutes of Health Research

HSREB Amendment Approval Date: June 24, 2014  
HSREB Expiry Date: September 30, 2016

Documents Approved and/or Received for Information:

Document Name	Comments	Version Date
Revised Western University Protocol		2014/05/15
Revised Letter of Information & Consent	version 6	2014/05/15

The Western University Health Science Research Ethics Board (HSREB) has reviewed and approved the amendment to the above named study, as of the HSREB Initial Approval Date noted above.

HSREB approval for this study remains valid until the HSREB Expiry Date noted above, conditional to timely submission and acceptance of HSREB Continuing Ethics Review. If an Updated Approval Notice is required prior to the HSREB Expiry Date, the Principal Investigator is responsible for completing and submitting an HSREB Updated Approval Form in a timely fashion.

The Western University HSREB operates in compliance with the Tri-Council Policy Statement Ethical Conduct for Research Involving Humans (TCPS2), the International Conference on Harmonization of Technical Requirements for Registration of Pharmaceuticals for Human Use Guideline for Good Clinical Practice Practices (ICH E6 R1), the Ontario Personal Health Information Protection Act (PHIPA, 2004), Part 4 of the Natural Health Product Regulations, Health Canada Medical Device Regulations and Part C, Division 5, of the Food and Drug Regulations of Health Canada.

Members of the HSREB who are named as investigators in research studies do not participate in discussions related to, nor vote on such studies when they are presented to the REB.

---

**Principal Investigator:** Dr. G. Parraga

**Review Number:** 13743

**Review Level:** Full Board

**Review Date:** November 6, 2007

**Protocol Title:** A single-centre pilot study exploring the utility of magnetic resonance imaging in patients with chronic lung disease

**Department and Institution:** Radiology, Robarts Research Institute

**Sponsor:**

**Ethics Approval Date:** November 27, 2007

**Expiry Date:** October 31, 2017

**Documents Reviewed and Approved:** UWO Protocol, Letter of Information and Consent dated November 16, 2007

**Documents Received for Information:** Protocol, October 23, 2007; IB, 6th ed, 09 Sept 2005

---

This is to notify you that The University of Western Ontario Research Ethics Board for Health Sciences Research Involving Human Subjects (HSREB) which is organized and operates according to the Tri-Council Policy Statement: Ethical Conduct of Research Involving Humans and the Health Canada/ICH Good Clinical Practice Practices: Consolidated Guidelines; and the applicable laws and regulations of Ontario has reviewed and granted approval to the above referenced study on the approval date noted above. The membership of this REB also complies with the membership requirements for REB's as defined in Division 5 of the Food and Drug Regulations.

The ethics approval for this study shall remain valid until the expiry date noted above assuming timely and acceptable responses to the HSREB's periodic requests for surveillance and monitoring information. If you require an updated approval notice prior to that time you must request it using the UWO Updated Approval Request Form.

During the course of the research, no deviations from, or changes to, the protocol or consent form may be initiated without prior written approval from the HSREB except when necessary to eliminate immediate hazards to the subject or when the change(s) involve only logistical or administrative aspects of the study (e.g. change of monitor, telephone number). Expedited review of minor change(s) in ongoing studies will be considered. Subjects must receive a copy of the signed information/consent documentation.

Investigators must promptly also report to the HSREB:

- a) changes increasing the risk to the participant(s) and/or affecting significantly the conduct of the study;
- b) all adverse and unexpected experiences or events that are both serious and unexpected;
- c) new information that may adversely affect the safety of the subjects or the conduct of the study.

If these changes/adverse events require a change to the information/consent documentation, and/or recruitment advertisement, the newly revised information/consent documentation, and/or advertisement, must be submitted to this office for approval.

Members of the HSREB who are named as investigators in research studies, or declare a conflict of interest, do not participate in discussion related to, nor vote on, such studies when they are presented to the HSREB.



Western  
Research

Western University Health Science Research Ethics Board  
HSREB Amendment Approval Notice

Research Ethics

Principal Investigator: Dr. Grace Parraga  
Department & Institution: Schulich School of Medicine and Dentistry/Imaging/Robarts Research Institute

HSREB File Number: 4819  
Study Title: A single-centre pilot study exploring the utility of magnetic resonance imaging in patients with chronic lung disease (REB #13743)  
Sponsor:

HSREB Amendment Approval Date: July 30, 2014  
HSREB Expiry Date: October 31, 2017

Documents Approved and/or Received for Information:

Document Name	Comments	Version Date
Revised Western University Protocol		2014/07/14
Revised Letter of Information & Consent		2014/07/14

The Western University Health Science Research Ethics Board (HSREB) has reviewed and approved the amendment to the above named study, as of the HSREB Initial Approval Date noted above.

HSREB approval for this study remains valid until the HSREB Expiry Date noted above, conditional to timely submission and acceptance of HSREB Continuing Ethics Review. If an Updated Approval Notice is required prior to the HSREB Expiry Date, the Principal Investigator is responsible for completing and submitting an HSREB Updated Approval Form in a timely fashion.

The Western University HSREB operates in compliance with the Tri-Council Policy Statement Ethical Conduct for Research Involving Humans (TCPS2), the International Conference on Harmonization of Technical Requirements for Registration of Pharmaceuticals for Human Use Guideline for Good Clinical Practice Practices (ICH E6 R1), the Ontario Personal Health Information Protection Act (PHIPA, 2004), Part 4 of the Natural Health Product Regulations, Health Canada Medical Device Regulations and Part C, Division 5, of the Food and Drug Regulations of Health Canada.

Members of the HSREB who are named as investigators in research studies do not participate in discussions related to, nor vote on such studies when they are presented to the REB.

---

**Principal Investigator:** Dr. G. Parraga  
**Review Number:** 15930 **Review Level:** Full Board  
**Review Date:** February 10, 2009  
**Protocol Title:** Longitudinal Study of Helium-3 Magnetic Resonance Imaging of COPD  
**Department and Institution:** Diagnostic Radiology & Nuclear Medicine, Robarts Research Institute  
**Sponsor:** INTERNAL RESEARCH FUND-UWO  
**Ethics Approval Date:** May 25, 2009 **Expiry Date:** November 30, 2013  
**Documents Reviewed and Approved:** UWO Protocol, Letter of information & consent form for Patients dated March 26/09 & Letter of information & consent form for Healthy Volunteers dated March 26/09  
**Documents Received for Information:** Protocol, January 27, 2009; IB, ed 6, 09 Sep. 05

---

This is to notify you that The University of Western Ontario Research Ethics Board for Health Sciences Research Involving Human Subjects (HSREB) which is organized and operates according to the Tri-Council Policy Statement: Ethical Conduct of Research Involving Humans and the Health Canada/ICH Good Clinical Practice Practices: Consolidated Guidelines; and the applicable laws and regulations of Ontario has reviewed and granted approval to the above referenced study on the approval date noted above. The membership of this REB also complies with the membership requirements for REB's as defined in Division 5 of the Food and Drug Regulations.

The ethics approval for this study shall remain valid until the expiry date noted above assuming timely and acceptable responses to the HSREB's periodic requests for surveillance and monitoring information. If you require an updated approval notice prior to that time you must request it using the UWO Updated Approval Request Form.

During the course of the research, no deviations from, or changes to, the protocol or consent form may be initiated without prior written approval from the HSREB except when necessary to eliminate immediate hazards to the subject or when the change(s) involve only logistical or administrative aspects of the study (e.g. change of monitor, telephone number). Expedited review of minor change(s) in ongoing studies will be considered. Subjects must receive a copy of the signed information/consent documentation.

Investigators must promptly also report to the HSREB:

- a) changes increasing the risk to the participant(s) and/or affecting significantly the conduct of the study;
- b) all adverse and unexpected experiences or events that are both serious and unexpected;
- c) new information that may adversely affect the safety of the subjects or the conduct of the study.

If these changes/adverse events require a change to the information/consent documentation, and/or recruitment advertisement, the newly revised information/consent documentation, and/or advertisement, must be submitted to this office for approval.

Members of the HSREB who are named as investigators in research studies, or declare a conflict of interest, do not participate in discussion related to, nor vote on, such studies when they are presented to the HSREB.



Western  
Research

Western University Health Science Research Ethics Board  
HSREB Amendment Approval Notice

Research Ethics

Principal Investigator: Dr. Grace Pantaga  
Department & Institution: Schulich School of Medicine and Dentistry/Imaging, Roberts Research Institute

HSREB File Number: 6014  
Study Title: Longitudinal Study of Helium-3 Magnetic Resonance Imaging of COPD (REB #1590)  
Sponsor: UWO Internal Research Fund

HSREB Amendment Approval Date: July 30, 2014  
HSREB Expiry Date: March 31, 2018

Documents Approved and/or Received for Information:

Document Name	Comments	Version Date
Revised Western University Protocol		2014/07/07
Revised Letter of Information & Consent	version 12	2014/07/07

The Western University Health Science Research Ethics Board (HSREB) has reviewed and approved the amendment to the above named study, as of the HSREB Initial Approval Date noted above.

HSREB approval for this study remains valid until the HSREB Expiry Date noted above, conditional to timely submission and acceptance of HSREB Continuing Ethics Review. If an Updated Approval Notice is required prior to the HSREB Expiry Date, the Principal Investigator is responsible for completing and submitting an HSREB Updated Approval Form in a timely fashion.

The Western University HSREB operates in compliance with the Tri-Council Policy Statement Ethical Conduct for Research Involving Humans (TCPS2), the International Conference on Harmonization of Technical Requirements for Registration of Pharmaceuticals for Human Use Guideline for Good Clinical Practice Practices (ICH E6 R1), the Ontario Personal Health Information Protection Act (PHIPA, 2004), Part 4 of the Natural Health Product Regulations, Health Canada Medical Device Regulations and Part C, Division 5, of the Food and Drug Regulations of Health Canada.

Members of the HSREB who are named as Investigators in research studies do not participate in discussions related to, nor vote on such studies when they are presented to the REB.

## Appendix C - Curriculum Vitae

### EDUCATION

- 2015-** Master of Science in Medical Biophysics (*Candidate*)  
Department of Medical Biophysics  
**The University of Western Ontario, London, Canada**  
*Supervisor: Dr. Grace Parraga*
- 2015** Bachelor of Science (Honours Physics)  
Minor in Psychology  
Department of Physics  
**The University of Windsor, Windsor, Canada**  
*Supervisor: Dr. Roman G. Maev*

### POSITIONS

- 2015-** **Robarts Research Institute  
London, Ontario**  
Graduate Research Assistant, MSc Candidate  
Department of Medical Biophysics, The University of Western Ontario  
*Supervisor: Dr. Grace Parraga*
- 2015** **Robarts Research Institute  
London, Ontario**  
Summer Student  
*Supervisor: Dr. Grace Parraga*
- 2013-2015** **Institute for Diagnostic Imaging Research  
Windsor, Ontario**  
Undergraduate Research Assistant  
*Supervisor: Dr. Roman G. Maev*

### HONOURS AND AWARDS

- 2015 -** **Western Graduate Research Scholarship**  
Department of Medical Biophysics, The University of Western Ontario  
*Awarded to a full time graduate student for stipend support who has maintained an average of 80% or more.*  
Institutional (\$1,500 per term)
- 2016** **Educational Stipend Award**  
***International Society for Magnetic Resonance in Medicine***  
*Awarded to support the attendance of students, postdoctoral and clinical trainees to present abstracts at the scientific meeting.*  
International (\$475 USD)

### PUBLICATIONS AND PRESENTATIONS

#### A Peer-Reviewed Journal Manuscripts

##### **Published (2)**

1. A Ouriadov, **E Lessard**, K Sheikh and G Parraga. Pulmonary MRI Morphometry Modelling of Airspace Enlargement in Chronic Obstructive Pulmonary Disease and Alpha-1 Antitrypsin Deficiency, *Magn Reson Med*, doi: 10.1002/mrm.26642 [Epub ahead of print]

2. G Paulin, A Ouriadov, **E Lessard**, K Sheikh, DG McCormack and G Parraga. Non-Invasive Quantification of Alveolar Morphometry in Elderly Never- and Ex-Smokers *Physiol Rep*, 3 (10), 2015, e12583, doi: 10.14814/phy2.12583

#### **Accepted with revisions (1)**

1. **E Lessard**, HM Young, A Bhalla, D Pike, K Sheikh, DG McCormack, A Ouriadov and G Parraga. Pulmonary Magnetic Resonance Imaging Biomarkers of Regional Airspace Enlargement in Alpha-1 Antitrypsin Deficiency, *Accepted with revisions to Acad Radiol April 21, 2017*

#### **B Proffered Oral Presentations (3)**

1. **E Lessard**, A Ouriadov, DPI Capaldi, DG McCormack and G Parraga, Novel Biomarkers of Lung Parenchyma Destruction and Emphysema Progression in COPD Using Inhaled Gas MRI Morphometry. American Thoracic Society Annual Scientific Meeting 2016 San Francisco CA May 13-18, 2016
2. A Ouriadov, **E Lessard**, DG McCormack and G Parraga, Can the Stretched Exponential Model of Gas Diffusion Provide Clinically-Relevant Parenchyma Measurements of Lung Disease? International Society of Magnetic Resonance in Medicine Annual Scientific Meeting 2016 Suntec City, Singapore May 7-13, 2016.
3. A Ouellette, **E Lessard**, AM Chertov, RG Maev. Real Time 2D Imaging of the Spot Weld Process, The American Society for Non-destructive Testing 23rd Research Symposium, March 27, 2014, Las Vegas, NV

#### **C Invited and Proffered Poster Presentations (9)**

1. A Ouriadov, **E Lessard**, F Guo, HM Young, A Bhalla, DG McCormack and G Parraga. Accelerated Diffusion-weighted <sup>129</sup>Xe MRI Morphometry of Emphysema. Imaging Network of Ontario (ImNO), 15<sup>th</sup> Annual Imaging Network Ontario Symposium, London, Canada, March 15-16, 2016.
2. A Ouriadov, **E Lessard**, F Guo, HM Young, A Bhalla, HO Coxson, DG McCormack and G Parraga. Biomarkers of Emphysema in COPD and Alpha-1 Antitrypsin Deficiency: <sup>129</sup>Xe MRI Morphomics. American Thoracic Society Annual Scientific Meeting 2017 Washington DC May 19-24, 2017.
3. A Ouriadov, **E Lessard**, F Guo, HM Young, A Bhalla, DG McCormack and G Parraga. Accelerated Diffusion-weighted <sup>129</sup>Xe MRI Morphometry of Emphysema in COPD and Alpha-1 Antitrypsin Deficiency Patients. International Society of Magnetic Resonance in Medicine Annual Scientific Meeting Honolulu, HI April 22-27, 2017.
4. **E Lessard**, A Bhalla, A Ouriadov, D Pike, DG McCormack and G Parraga, Longitudinal Three-Year Decline in Alpha-1 Antitrypsin Deficiency: Regional Worsening in Emphysema and Ventilation. Roberts Research Retreat 2016 London, Canada, June 13, 2016.
5. **E Lessard**, A Ouriadov, DG McCormack and G Parraga, Single Compartment model estimates of acinar duct measurements from inhaled noble gas MRI: Proof of Concept in alpha-1 antitrypsin deficiency emphysema. London Health Research Day 2016 London, Canada March 29, 2016.
6. A Bhalla, A Ouriadov, **E Lessard**, DG McCormack and G Parraga, Longitudinal MRI Morphomics: towards an understanding of response to therapy and disease progression in patients with Alpha-1 Antitrypsin Deficiency pulmonary emphysema. London Health Research Day 2016 London, Canada March 29, 2016. (Top 100 Poster)
7. **E Lessard**, A Ouriadov, DG McCormack and G Parraga, Single Compartment model estimates of acinar duct measurements from inhaled noble gas MRI: Proof of Concept in alpha-1 antitrypsin deficiency emphysema. International Society of Magnetic Resonance in Medicine Annual Scientific Meeting 2016 Suntec City, Singapore May 7-13, 2016.
8. **E Lessard**, A Bhalla, A Ouriadov, D Pike, DG McCormack and G Parraga, Longitudinal Three-Year Decline in Alpha-1 Antitrypsin Deficiency: Regional Worsening in Emphysema and Ventilation. American Thoracic Society Annual Scientific Meeting 2016 San Francisco CA May 13-18, 2016.

9. A Ouriadov, **E Lessard**, DG McCormack, G Parraga. Single-breath  $^3\text{He}$  Whole Lung Morphometry in Alpha-1 Antitrypsin Deficiency: Towards an Understanding of Parenchymal Destruction and Response to Treatment. International Workshop for Pulmonary Functional Imaging Edinburgh, UK September 30th, 2015

## **D Academic Reports**

1. **E Lessard**, Investigation of Magnetic Field and Current Based Triggers for Use in the Ultrasonic Monitoring of the Resistance Spot Weld Process. *University of Windsor Undergraduate Thesis*, Windsor, Ontario, 2014

## **COMMITTEES AND PROFESSIONAL ACTIVITIES**

**2013-2015 University of Windsor**  
Undergraduate Representative  
Department of Physics

## **PROFESSIONAL SOCIETIES**

**2015-2017** American Thoracic Society  
*Student Member*

**2015-2017** Canadian Thoracic Society  
*Student Member*

**2015-2017** Canadian Organization of Medical Physicists  
*Student Member*

**2015-** International Society for Magnetic Resonance in Medicine  
*Student Member*

**2014-2016** Canadian Association of Physicists  
*Student Member*

**2010-2016** American Physical Society  
*Student Member*

## **ACADEMIC RESPONSIBILITIES**

### **Undergraduate Teaching**

**2014-2015** **Introductory Physics II (University of Windsor: 03-64-141)**  
-Proctored Exams and Laboratory Instructor (2h Lab, 1h Tutorial per week)

**Introduction to Astronomy II (University of Windsor: 03-64-191)**  
-Proctored Exams and marked group projects.

**Introductory Physics I (University of Windsor: 03-64-140)**  
-Proctored Exams, marked midterm and final exam.

## **LEADERSHIP, VOLUNTEER and COMMUNITY ACTIVITIES**

**2016-2017** **Research Assistant Volunteer**, Canadian Alliance for Healthy Hearts & Minds, Population Health Research Institute  
Administered Montreal Cognitive Assessments (MoCa) and Digital Substitution Exercises. Obtained volunteer physical measurements. Responsible for using DataFax software.

**2015-** **Volunteer**, London Powerlifting Club, Ontario Powerlifting Association

**2014-2015** **Vice President**, Physics Club, University of Windsor

**2014** **Volunteer**, Science Academy, University of Windsor

**2013-2014** **Junior Vice President**, Physics Club, University of Windsor

**2013** **Volunteer**, Science Rendezvous, University of Windsor